CDK1 depletion suppresses glioma malignancy through cell cycle pathway regulation: Mechanistic insights from functional and molecular profiling

YU WANG[1*], HUANDI ZHOU[1-3*], XUETAO HAN[1,2], DONGDONG ZHANG[1,4], LIUBING HOU[1,3], HAONAN LI[1], TIANYI FAN[1], SIJIE LI[1] and XIAOYING XUE[1,2]

[1]Department of Radiotherapy, The Second Hospital of Hebei Medical University, Shijiazhuang, Hebei 050000, P.R. China; [2]Hebei Key Laboratory of Etiology Tracing and Individualized Diagnosis and Treatment for Digestive System Carcinoma, Shijiazhuang, Hebei 050000, P.R. China; [3]Department of Central Laboratory, The Second Hospital of Hebei Medical University, Shijiazhuang, Hebei 050000, P.R. China; [4]Department of Oncology, Hefei-Cancer Hospital, Chinese Academy of Sciences, Hefei, Anhui 230031, P.R. China

Received August 21, 2025; Accepted November 6, 2025

DOI: 10.3892/or.2026.9046

Abstract. Glioblastoma remains a lethal malignancy with limited therapeutic advancements. Emerging evidence implicates cell cycle dysregulation in glioma pathogenesis, yet the mechanistic role of cyclin-dependent kinase 1 (CDK1) remains underexplored. The present study systematically evaluated the clinical relevance and functional impact of CDK1 in glioma progression through multi-modal experimental approaches. CDK1 expression was analyzed using public datasets and then verified by western blotting using patient tissue samples (n=37) from the Second Hospital of Hebei Medical University (Shijiazhuang, China). Survival analysis was performed using Chinese Glioma Genome Atlas and The Cancer Genome Atlas datasets, alongside multivariate Cox regression to evaluate prognostic independence. Functional assays, including small interfering RNA-mediated CDK1 knockdown, were conducted in glioma cell lines to assess proliferation (Cell Counting Kit-8 and EdU), migration/invasion (Transwell), apoptosis (acridine orange/ethidium bromide staining and flow cytometry) and radiosensitivity (γ-H2AX foci quantification post-irradiation). The expression levels of downstream cell cycle regulators were quantified via quantitative PCR. The results indicated that CDK1 was significantly upregulated in glioma tissues compared with normal controls, with expression levels escalating with tumor grade. High CDK1 expression correlated with a reduced overall survival and served as an independent prognostic marker. CDK1 knockdown attenuated glioma cell proliferation, migration and invasion, while enhancing apoptosis and radiosensitivity. Mechanistically, CDK1 knockdown downregulated cell cycle regulators proliferating cell nuclear antigen, minichromosome maintenance complex component 2-4 (MCM2-4), MCM6, polo-like kinase 1, TTK protein kinase and mitotic arrest deficient 2 like 1, implicating mitotic dysregulation as a central pathway. The present study established CDK1 as a master regulator of glioma progression through coordinated control of proliferation, DNA repair and metastatic potential. The robust association between CDK1 expression, tumor grade and survival, coupled with functional validation across complementary assays, positions CDK1 inhibition as a promising therapeutic strategy. The mechanistic elucidation of its cell cycle network provides a novel framework for targeting glioma-specific therapeutic targets.

Correspondence to: Professor Xiaoying Xue, Department of Radiotherapy, The Second Hospital of Hebei Medical University, 215 Heping West Road, Xinhua, Shijiazhuang, Hebei 050000, P.R. China
E-mail: xxy0636@hebmu.edu.cn

*Contributed equally

Abbreviations: GEO, Gene Expression Omnibus; DEGs, differentially expressed genes; PPI, protein-protein interaction; HPA, Human Protein Atlas; GEPIA, Gene Expression Profiling Interactive Analysis; CGGA, Chinese Glioma Genome Atlas; TCGA, The Cancer Genome Atlas; GSEA, Gene Set Enrichment Analysis; CDK1, cyclin-dependent kinase 1; PCNA, proliferating cell nuclear antigen; PLK1, polo-like kinase 1; MCM2/3/4/6, minichromosome maintenance complex component 2/3/4/6; TTK, TTK protein kinase; MAD2L1, mitotic arrest deficient 2 like 1; IDH, isocitrate dehydrogenase; MGMT, O-6-methylguanine-DNA methyltransferase; CDKN2A, cyclin dependent kinase inhibitor 2A; FDR, false discovery rate; NES, normalized enrichment score; EMT, epithelial-mesenchymal transition; DSB, double-strand break; CtIP, CtBP-interacting protein; OS, overall survival; ROC, receiver operating characteristic; AUC, area under the curve; WHO, World Health Organization; OD, optical density; NC, negative control; si, small interfering (RNA); AO/EB, acridine orange/ethidium bromide; GBM, glioblastoma; LGG, low-grade glioma

Keywords: glioma, CDK1, cell cycle, DNA repair, molecular target

Introduction

Gliomas are among the most common primary malignant tumors of the central nervous system (CNS), arise from glial or neural precursor cells and encompass histological

subtypes such as astrocytoma [including glioblastoma (GBM)], oligodendroglioma, ependymoma and oligoastrocytoma [now classified as glioma, isocitrate dehydrogenase (IDH)-mutant] (1). GBM, the most aggressive glioma subtype, poses major therapeutic challenges due to its highly malignant phenotype and poor prognosis. Despite significant advances in anticancer therapies, including immunotherapy, GBM remains largely unresponsive to conventional and novel interventions. The limited efficacy of immunotherapy in GBM primarily stems from its notably immunosuppressive tumor microenvironment and intrinsic resistance mechanisms (2,3). The 2016 World Health Organization (WHO) Classification of Tumors of the CNS marked a paradigm shift by integrating molecular biomarkers into diagnostic criteria (4). The 2021 fifth edition of the WHO CNS classification further refined this framework, establishing histomolecular classification as a cornerstone of modern neuro-oncology (5). Key molecular biomarkers include IDH mutations, 1p/19q codeletion, H3F3A alterations, α thalassemia/mental retardia syndrome X-linked mutations, O^6-methylguanine-DNA methyltransferase (MGMT) promoter methylation, cyclin dependent kinase inhibitor 2A (CDKN2A) homozygous deletion, epidermal growth factor receptor amplification, combined chromosome 7 gain/chromosome 10 loss (7+/10-) and telomerase reverse transcriptase promoter mutations (5,6). In adults, IDH mutation status and MGMT promoter methylation serve as strong prognostic indicators for glioma, while CDKN2A homozygous deletion is a critical marker of histological progression in IDH-mutant astrocytomas (7). Recent discoveries have expanded the molecular landscape of glioma. For instance, olfactomedin like 3 has emerged as a biomarker associated with poor prognosis; its knockdown enhances temozolomide sensitivity and may reflect immune dysregulation within the tumor microenvironment (8). Such findings underscore the pivotal role of comprehensive molecular profiling in enabling precise glioma classification and personalized therapy development. Beyond molecular characterization, integrating multimodal data, including radiological, histopathological and genomic modalities, has shown promise for improving prognostic accuracy and deep learning frameworks capable of jointly analyzing these data types consistently outperform single-modality approaches (9). Notably, Yuan *et al* (10) developed a squeeze-and-excitation deep learning model that integrated preoperative T1-contrast-enhanced MRI, digitized whole-slide histopathological images and circulating 5-hydroxymethylcytosine profiles, achieving a marked prognostic performance (concordance index=0.897) in a glioma cohort. By effectively capturing glioma heterogeneity across spatial and temporal dimensions, such multimodal strategies represent a significant advance toward precision medicine in neuro-oncology. Current standard management involves maximal safe surgical resection followed by adjuvant radiotherapy with concurrent temozolomide chemotherapy, typically initiated within 30 days postoperatively (11). Although emerging molecular-targeted therapies and immunotherapies have shown promise in select molecular subtypes, most patients with glioma experience limited clinical benefit due to inadequate target specificity, restricted blood-brain barrier permeability, acquired resistance and dose-limiting toxicities (12,13). Consequently, continued discovery of novel molecular markers remains essential to elucidate gliomagenesis mechanisms, identify actionable targets and accelerate the translation of precision medicine in glioma therapy.

The cyclin-dependent kinase (CDK) family plays a pivotal role in regulating signaling pathways that govern transcriptional control and cell cycle progression. Within the cell cycle, CDK2, CDK4 and CDK6 coordinate interphase progression, whereas CDK1 orchestrates mitotic entry (14). As a key G2/M checkpoint kinase (15), CDK1 drives tumor proliferation and survival across multiple malignancies, including breast, colorectal and lung cancer (16-19). Clinically, elevated CDK1 expression serves as a prognostic biomarker strongly associated with poor oncological outcomes, including in colorectal, ovarian, breast and pancreatic cancer (20-24). The key regulators of the cell cycle, including proliferating cell nuclear antigen (PCNA), minichromosome maintenance complex component 2-4 (MCM2-4), MCM6, polo-like kinase 1 (PLK1), TTK protein kinase (TTK) and mitotic arrest deficient 2 like 1 (MAD2L1), collectively ensure DNA replication and mitotic fidelity (25,26). However, the functional relationship between CDK1 and these regulators remains to be fully elucidated. Therefore, systematically investigating the molecular mechanisms of CDK1 in glioma is of significant importance (27-29).

Materials and methods

Microarray data download. Gene expression datasets and associated clinical data (accession nos. GSE29796, GSE4290, GSE50161 and GSE7696) were retrieved from the Gene Expression Omnibus (GEO; https://www.ncbi.nlm.nih.gov/geo/). The GSE29796 dataset comprises 52 glioma specimens and 20 non-tumoral controls (30); GSE4290 includes 153 glioma and 23 non-tumoral samples (31); GSE50161 contains 117 glioma and 13 non-tumoral samples (32); and GSE7696 includes 80 glioma and 4 non-tumoral specimens (33). Additional datasets [mRNAseq_693 and mRNAseq_325 (34) were obtained from the Chinese Glioma Genome Atlas (CGGA; http://www.cgga.org.cn/), encompassing RNA sequencing profiles and clinical annotations for 1,018 glioma cases, along with RNA sequencing data from 20 non-tumoral brain tissues. For independent validation, RNA sequencing data and clinical information from 592 glioma specimens [449 low-grade glioma (LGG) and 143 GBM] were acquired from The Cancer Genome Atlas (TCGA; https://portal.gdc.cancer.gov/; TCGA-LGG and TCGA-GBM datasets; dbGaP accession phs000178) (35,36). Samples lacking complete clinical annotations were excluded. To minimize batch effects and technical variability, RNA sequencing data were normalized using the 'limma' package of Sangerbox 3.0 (http://sangerbox.com/) and log2 (x + 1) transformed before analysis.

Acquisition of tissue samples from 37 patients. Paired tumor specimens and histologically normal adjacent tissues (collected >2 cm from the tumor margin) were obtained from 37 patients with histologically confirmed glioma treated at the Department of Neurosurgery, The Second Hospital of Hebei Medical University (Shijiazhuang, China). Patient recruitment and sample collection spanned the period from August 2019 to December 2024. The enrolled cohort consisted of patients aged between 30 and 78 years, with a male-to-female ratio of

1.3:1. The inclusion criteria were as follows: i) Age ≥18 years; ii) patients who underwent surgical resection for primary brain tumors at the Second Hospital of Hebei Medical University; iii) initial diagnosis of glioma based on preoperative MRI findings and subsequent histopathological confirmation following surgical resection; iv) no prior history of radiotherapy or chemotherapy; and v) provision of written informed consent by the patient or their legal guardian. Patients were excluded from the study if they met any of the following criteria: i) Diagnosis of other intracranial tumors (such as meningioma and metastasis); ii) history of any other malignant tumors; iii) presence of severe cardiac, hepatic or renal dysfunction; iv) receipt of any preoperative anticancer therapy; and v) inadequate tissue sample quality for subsequent analysis. All collected specimens were immediately snap-frozen in liquid nitrogen post-resection and stored at -80˚C until analysis for CDK1 protein expression. The study protocol was reviewed and approved by the Ethics Committee of the Second Hospital of Hebei Medical University (Shijiazhuang, China; approval no.2019-R191) and all procedures were conducted in accordance with the principles of the Declaration of Helsinki.

Protein sample extraction. Frozen glioma and matched non-tumoral tissues were retrieved from -80˚C storage, thawed on ice and homogenized in radioimmunoprecipitation assay (RIPA) lysis buffer (Beijing Solarbio Science & Technology Co., Ltd.; cat. no. R0010) supplemented with phosphatase inhibitor cocktail (Beijing Solarbio Science & Technology Co., Ltd.; cat. no. P1260) using a tissue grinder. Homogenates were centrifuged at 10,000 x g for 10 min at 4˚C, then the supernatants were collected into fresh microcentrifuge tubes. Protein preparation from U251MG and LN229 cell lines was conducted by placing the processed cells on ice, adding the aforementioned RIPA buffer containing protein and phosphatase inhibitors. Lysis was performed on a rocking platform for 15 min. Protein concentrations were quantified using a BCA assay kit (Beijing Solarbio Science & Technology Co., Ltd.; cat. no. PC0020) and lysates were denatured at 100˚C for 15 min in loading buffer (Beijing Solarbio Science & Technology Co., Ltd.; cat. no. P1019).

Cell culture. The U251MG and LN229 human glioma cell lines were obtained from the China Infrastructure of Cell Line Resources, Institute of Basic Medical Sciences, Chinese Academy of Medical Sciences (Beijing, China). Cells were maintained in Dulbecco's Modified Eagle Medium (DMEM; Gibco; Thermo Fisher Scientific, Inc.; cat. no. 11995065) supplemented with 10% fetal bovine serum (FBS; Gibco; Thermo Fisher Scientific, Inc.; cat. no. A5670801) and 1% penicillin-streptomycin solution (Beijing Solarbio Science & Technology Co., Ltd.; cat. no. P1400) and incubated at 37˚C in a humidified atmosphere containing 5% CO_2.

Searching for genes involved in glioma initiation and progression. For differential expression analysis, the GSE29796, GSE4290, GSE50161 and GSE7696 datasets were divided into tumor and non-tumor groups. Differentially expressed genes (DEGs) were identified based on adjusted P<0.05 and $|\log_2$ fold change (FC)|>1 criteria. Volcano plots for each dataset were generated using the 'limma' package in R v4.0.5 (37). The jvenn online tool (http://jvenn.toulouse.inra.fr/app/usermanual.html) identified 360 consensus DEGs co-expressed across all four datasets. These DEGs were imported into the Search Tool for the Retrieval of Interacting Genes (STRING; https://string-db.org/) to construct a protein-protein interaction (PPI) network, excluding nodes with an interaction confidence score of <0.7 and isolated proteins. The resulting PPI network, containing 180 proteins, was visualized using Cytoscape (v3.7.2; https://cytoscape.org/). The cytoHubba plugin identified CDK1 as the hub gene based on maximal degree centrality.

CDK1 gene expression analysis. CDK1 expression in glioma and non-tumoral samples from the four GEO datasets (GSE29796, GSE4290, GSE50161 and GSE7696) was analyzed using the unpaired t-test for parametric data or the Mann-Whitney U test for non-parametric data in GraphPad Prism 8 (Dotmatics). Expression validation in GBM and LGG was further conducted using the Gene Expression Profiling Interactive Analysis (GEPIA; http://gepia.cancer-pku.cn/) and Human Protein Atlas (HPA; https://www.proteinatlas.org/) databases. Experimental validation of CDK1 expression was performed via western blotting under standardized conditions.

Correlation analysis of CDK1 expression level with clinical information and pathological features. The CGGA dataset comprising mRNA transcriptome data and clinical information from 1,018 glioma samples was used to assess associations between CDK1 expression and clinical prognosis, with findings validated using TCGA data. Samples were stratified into high- and low-expression groups based on median CDK1 expression levels. Kaplan-Meier survival analyses were performed using R v4.0.5 with the 'survival' and 'survminer' packages, while time-dependent receiver operating characteristic (ROC) curves at 1-, 3- and 5-year intervals were generated using the 'survivalROC' package. Univariate and multivariate Cox regression analyses were used to identify independent prognostic factors (significance threshold: P<0.001). Based on CGGA data, nomograms predicting 1-, 2- and 3-year survival probabilities were constructed using the 'survival' and 'rms' packages (R; v4.0.5), and calibration curves were used to assess the predictive accuracy. Finally, based on the CGGA data, associations between CDK1 expression and clinicopathological characteristics were analyzed using the 'beeswarm' package in R (v3.6.3). P<0.05 was considered to indicate a statistically significant difference for all analyses.

Western blotting. Denatured proteins (described above) from 37 paired glioma and adjacent normal tissues, as well as the U251MG and LN229 cell lines, were separated by electrophoresis on 10% SDS-polyacrylamide gels (an equal amount of 30 μg was loaded per lane) at a constant voltage of 120 V for 90 min and transferred to 0.45 μm PVDF membranes (Merck KGaA; cat. no. IPVH00010). Membranes were blocked with 5% (w/v) non-fat dry milk in Tris-buffered saline containing 0.1% Tween-20 (TBST) at 25˚C for 1 h. The membranes were incubated overnight at 4˚C with the following primary antibodies diluted in blocking buffer: Anti-CDK1 (34 kDa; 1:500; Proteintech Group, Inc.; cat. no. 19532-1-AP) and β-actin (42 kDa; 1:10,000; Proteintech Group, Inc.;

cat. no. 66009-1-Ig). Following three 10-min washes with TBST at 25˚C, the membranes were incubated for 1 h at 25˚C with HRP-conjugated goat anti-rabbit/mouse IgG (H+L) secondary antibodies (1:10,000; Proteintech Group, Inc.; cat. nos. SA00001-2 and SA00001-1). Protein bands were visualized using an ECL Western blotting kit (Biosharp Life Sciences; cat. no. BL520B) and detected via chemiluminescent imaging. Band intensities were semi-quantified using Image Lab software (v5.2.1; Bio-Rad Laboratories, Inc.).

CDK1 knockdown. CDK1-targeting small interfering RNAs (siRNAs) and the scrambled negative control (NC) were synthesized by Shanghai GenePharma Co., Ltd. The concentration of nucleic acid used was 20 pmol/μl. Transient transfection was performed using Lipofectamine 3000 (Thermo Fisher Scientific, Inc.; cat. no. L3000150) in U251MG and LN229 cells at 70-80% confluency, following the manufacturer's protocol. Transfection efficiency was verified by western blotting 48 h post-transfection. The effective siRNA duplex sequences were: CDK1, 5'-CCUAUGGAGUUGUGUAUA AGGTT-3' (sense) and 5'-CCUUAUACACAACUCCAUAGG TT-3' (anti-sense); and NC, 5'-UUCUCCGAACGUGUCACG UTT-3' (sense) and 5'-ACGUGACACGUUCGGAGAATT-3' (anti-sense).

Cell Counting Kit (CCK)-8 assay. Cell viability in the U251MG and LN229 cell lines was assessed using CCK-8 (MedChemExpress; cat. no. HY-K0301) according to the manufacturer's instructions. Cells were seeded in 96-well plates at $3x10^3$ cells/well in 100 μl of complete medium and allowed to adhere for 24 h. The medium was replaced with 110 μl of serum-free medium containing 10% (v/v) CCK-8 reagent, and plates were incubated for 1 h at 37˚C. Absorbance at 450 nm was recorded daily for 7 consecutive days using a NanoQuant spectrophotometer (Tecan Group, Ltd.). Data were collected from triplicate wells in three independent experiments.

EdU cell proliferation assay. U251MG and LN229 cells were seeded in 96-well plates at $1x10^4$ cells/well in 200 μl complete medium and cultured at 37˚C with 5% CO_2 for 24 h. Following the manufacturer's instructions (EdU Kit; Shanghai Yeasen Biotechnology Co., Ltd.; cat. no. 40276ES60), cells were incubated with 25 μM EdU in serum-free medium for 2 h at 37˚C. After fixation with 4% paraformaldehyde (PFA) for 30 min at 25˚C and permeabilization with 0.2% Triton X-100 for 20 min, cells were washed three times with phosphate-buffered saline (PBS). EdU was detected using Apollo 594 fluorescent dye (1:100 dilution) for 30 min in the dark, followed by nuclear counterstaining with Hoechst 33342 (1 μg/ml) for 10 min. Proliferating cells were visualized using an inverted fluorescence microscope (Leica DMi8) at x200 magnification. The proliferation index was calculated as the ratio of EdU-positive cells to total Hoechst 33342-stained nuclei.

Wound healing assay. U251MG cells were seeded in 6-well plates at $5x10^5$ cells/well and cultured to 70-80% confluency in a humidified incubator (37˚C, 5% CO_2). Linear scratches were created using a sterile 200 μl pipette tip and initial wound widths were recorded under a phase-contrast microscope. After three PBS washes (pH 7.4), cells were maintained in serum-free DMEM supplemented with 1% penicillin-streptomycin. Wound closure was monitored and imaged at 0, 24, 48 and 72 h post-scratch to evaluate the cell migration rates. The cell migration rate (%) was then calculated for each time point using the following formula based on the wound width: Migration rate=[(width at 0 h-width at T h)/width at 0 h] x100%, where T represents the specific time point after scratching.

Acridine orange/ethidium bromide (AO/EB) assay. U251MG and LN229 cells were seeded in 24-well plates at $5x10^4$ cells/well in 500 μl complete medium and incubated at 37˚C with 5% CO_2 for 24 h. After aspirating the medium and washing twice with PBS (pH 7.4), cells were stained following the manufacturer's protocol (AO/EB Staining Kit; Sangon Biotech Co., Ltd.; cat. no. E607308). Briefly, 200 μl AO/EB working solution was added per well, and cells were incubated in the dark at room temperature for 5 min. Fluorescence images were captured using an inverted fluorescence microscope (TRITC filter; x200 magnification). The apoptotic index was calculated as (EB^+ cells/total cells) x100%, based on three random fields per well. Data are from three biological replicates.

Transwell assay. U251MG and LN229 cells were serum-starved in DMEM for 24-48 h to promote migratory activation. Subsequently, $3x10^4$ treated cells were resuspended in serum-free DMEM and seeded into the upper chamber of 8 μm pore Transwell inserts (Corning, Inc.), either uncoated (migration assay) or coated with Matrigel (invasion assay). The Matrigel coating was performed by incubating a 1:8 dilution of Matrigel at 37˚C for 4 h to form a thin layer simulating the extracellular matrix. The lower chamber contained 500 μl of DMEM supplemented with 10% FBS as a chemoattractant. After 24-48 h incubation, cells were fixed with 4% PFA for 15 min at 25˚C and stained with 0.5% crystal violet for 20 min at 25˚C. Non-migrated cells on the upper surface were removed with a cotton swab, and the migrated/invaded cells on the lower surface were imaged under a light microscope.

Flow cytometry. U251MG cells were harvested by trypsinization, centrifuged at 300 x g for 5 min at 4˚C, and resuspended in 1X binding buffer according to the manufacturer's instructions (Annexin V-FITC Apoptosis Kit; Shanghai Yeasen Biotechnology Co., Ltd.; cat. no. 40302ES08). The cells were subsequently stained with Annexin V-FITC and propidium iodide staining solution and incubated in the dark at room temperature for 10-15 min. Following staining, apoptotic rates were quantified using a flow cytometer (Canto II; BD Biosciences) in strict accordance with the kit protocol to ensure reproducibility. For statistical analysis, the proportion of cells within the Q2 quadrant was selected to represent apoptotic populations using FlowJo software (v10.8.1, FlowJo LLC; BD Biosciences).

γ-H2AX immunofluorescence assay. U251MG and LN229 cells were seeded in 8-well chamber slides at a density of $5x10^4$ cells per well in 300 μl of complete medium and cultured for 24 h at 37˚C under 5% CO_2. After exposure to 5 Gy X-irradiation, cells were fixed with ice-cold 4% paraformaldehyde for 30 min

at the specified time points (0.5, 2, 6 and 24 h post-irradiation). Permeabilization was performed using 0.2% Triton X-100 in PBS for 20 min at room temperature, followed by blocking with 2% BSA (Beijing Solarbio Science & Technology Co., Ltd.; cat no. A8010) for 1 h at 25˚C. For γ-H2AX foci detection, cells were incubated overnight at 4˚C with rabbit anti-γ-H2AX monoclonal antibody (1:200; Cell Signaling Technology, Inc.; cat. no. 9718S). After three 5-min PBS washes, Alexa Fluor 488-conjugated goat anti-rabbit IgG (1:200; Proteintech Group, Inc.; cat. no. SA00013-2) was applied for 1 h at room temperature in the dark. Nuclei were counterstained with DAPI (Abbkine Scientific Co., Ltd.; cat. no. BMU107) for 30 min at 25˚C. Fluorescent images were acquired using a confocal microscope, and γ-H2AX foci were quantified using ImageJ software (v2.3.0; National Institutes of Health).

Reverse transcription-quantitative PCR (RT-qPCR). Total RNA was isolated from glioma cells using TRIzol reagent (Invitrogen; Thermo Fisher Scientific, Inc.). cDNA synthesis was performed using Hifair® III 1st Strand cDNA Synthesis SuperMix (Shanghai Yeasen Biotechnology Co., Ltd.; cat. no. 11141ES60) according to the manufacturer's protocol. Briefly, the reaction mixture was incubated at 25˚C for 5 min, followed by reverse transcription at 55˚C for 15 min and final enzyme inactivation at 85˚C for 5 min. qPCR was carried out using Hieff UNICON® Universal Blue qPCR SYBR Green Master Mix (Shanghai Yeasen Biotechnology Co., Ltd.; cat. no. 11201ES08) on a Bio-Rad qPCR system (Bio-Rad Laboratories, Inc.). Thermal cycling conditions were as follows: Initial denaturation at 95˚C for 5 min, followed by 40 cycles of 95˚C for 10 sec (denaturation), 60˚C for 10 sec (annealing) and 72˚C for 20 sec (extension), ending with a final hold at 4˚C. Primer sequences were as follows: CDK1: 5'-CAGACTAGA AAGTGAAGAGGAAGG-3' (forward) and 5'-ACTGACCAG GAGGGATAGAATC-3' (reverse); MCM6: 5'-GAGGAACTG ATTCGTCCTGAGA-3' (forward) and 5'-CAAGGCCCGACA CAGGTAAG-3' (reverse); MCM3: 5'-CTGAAGGCGAGGAAT GTTGGTG-3' (forward) and 5'-GATGGGAAGTAGGGCGGA TGAG-3' (reverse); PLK1: 5'-CCTGCACCGAAACCGAGT TA-3' (forward) and 5'-TAGGAGTCCCACACAGGGTC-3' (reverse); MCM2: 5'-GTTCAGCGTCATGCGGAGTAT-3' (forward) and 5'-TCTCGCCGGAAGGAGAGATA-3' (reverse); MCM4: 5'-CAACGGCATCTGCTGTATCG-3' (forward) and 5'-CTGACAGATGATCCCAGCCTTT-3' (reverse); MAD2L1: 5'-ACGGTGACATTTCTGCCACT-3' (forward) and 5'-TGG TCCCGACTCTTCCCATT-3' (reverse); PCNA: 5'-TCGTCT CACGTCTCCTTGGT-3' (forward) and 5'-TTTTGGACATGC TGGTGAGGT-3' (reverse); GAPDH: 5'-TCATTTCCTGGT ATGACAACGA-3' (forward) and 5'-GTCTTACTCCTTGGA GGCC-3' (reverse). GAPDH served as the internal control for normalization and relative mRNA expression levels were calculated using the $2^{-\Delta\Delta Cq}$ method (38).

DEG analysis and pathway enrichment analysis of the CDK1 gene. To investigate the specific biological functions of the hub gene CDK1 in glioma, a subsequent and distinct DEG analysis was performed. Unlike the initial analysis aimed at discovering pan-glioma associated genes across multiple datasets (GSE29796, GSE4290, GSE50161 and GSE7696), this analysis focused on comparing transcriptional profiles between CDK1-high and CDK1-low expression groups within the CGGA glioma cohort. mRNA sequencing data from the CGGA glioma dataset were retrieved and normalized as aforementioned. Samples were divided into CDK1-high and CDK1-low groups based on the median CDK1 expression. DEGs were identified using thresholds of $P<0.05$ and $|\log_2 FC|>1$, resulting in 638 significant DEGs [false discovery rate (FDR)<0.05]. Volcano plots were generated using the limma package in R (v4.3.1) (37). To elucidate the functional implications of these DEGs, enrichment analyses were conducted. Gene Ontology (GO) enrichment was performed using Metascape (39) (https://metascape.org/), while Kyoto Encyclopedia of Genes and Genomes (KEGG) pathway enrichment was assessed via Sangerbox 3.0 (http://sangerbox.com/) using Gene Set Enrichment Analysis (GSEA). Gene sets were considered significantly enriched when normalized enrichment score (NES)>1, P<0.05 and FDR <0.05.

Association analysis between CDK1 and hub genes. GO and GSEA revealed a prominent association of CDK1 with mitotic cell cycle regulation in glioma. Genes involved in the cell cycle were intersected between the Metascape and GSEA datasets using a Venn diagram (http://jvenn.toulouse.inra.fr/app/usermanual.html). The 29 overlapping genes were imported into the STRING database (https://string-db.org/) to construct a high-confidence protein-protein interaction (PPI) network (interaction score >0.9; FDR <0.01). The resulting network was visualized in Cytoscape, and the top 8 hub proteins showing co-expression coefficients of >0.9 relative to CDK1 were identified. Spearman correlation analysis using the Sangerbox platform (http://sangerbox.com/) confirmed strong correlations ($\rho>0.65$) between CDK1 and these hub genes. Expression and survival analyses were subsequently performed for each hub gene using TCGA dataset, assessing their clinical relevance in glioma prognosis.

Statistical analysis. All experimental data were analyzed and visualized using R software (v4.2.2) and GraphPad Prism 8.0 (Dotmatics), respectively. Overall survival (OS) differences were assessed using the log-rank test and illustrated via Kaplan-Meier survival curves. The normality of the data distribution was assessed using the Shapiro-Wilk test prior to statistical comparisons. The statistical analysis of western blot data (from 37 paired glioma and adjacent normal tissues) was performed using the non-parametric Wilcoxon matched-pairs signed-rank test. Statistical comparisons between two independent groups (such as data derived from CDK1 mRNA expression in GEO datasets and the EdU, AO/EB, Transwell and apoptotic assays) were performed using the unpaired t-test for parametric data and the Mann-Whitney U test for non-parametric data. For comparisons among more than two groups under one independent variable (such as transfection efficiency validation across the Blank, NC and siRNA groups), one-way analysis of variance (ANOVA) with Tukey's post hoc test was used for parametric data, while the Kruskal-Wallis test followed by Dunn's post hoc test was applied to non-parametric data. In cases involving two independent variables (such as CCK-8 assay across days 1 to 7, wound healing assay at 0, 24, 48 and 72 h and the γ-H2AX assay at 0.5, 2, 6 and 24 h), a two-way ANOVA was used to assess main effects and

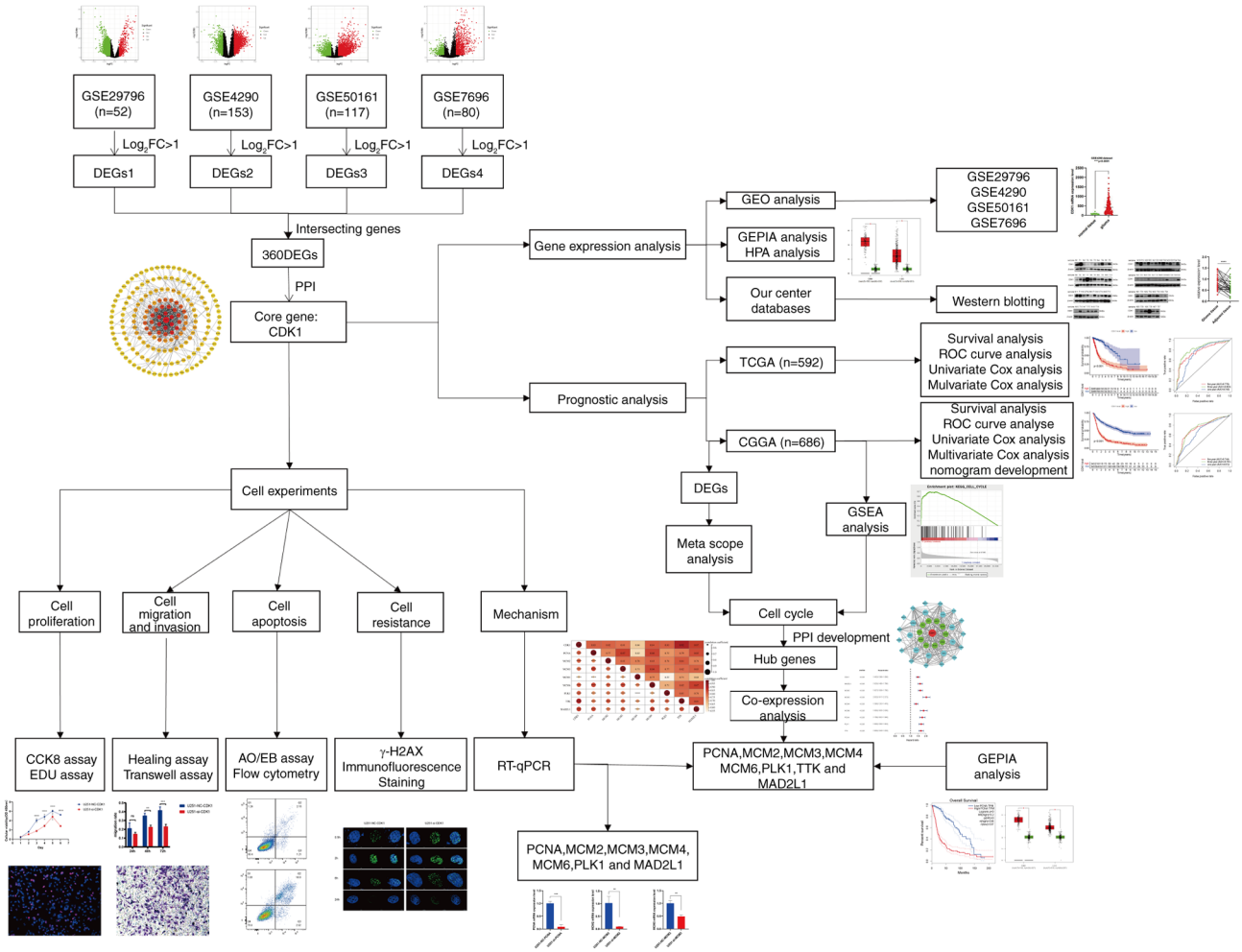

Figure 1. Workflow of the whole study. FC, fold change; DEGs, differentially expressed genes; CDK1, cyclin-dependent kinase 1; GEPIA, Gene Expression Profiling Interactive Analysis; N, normal tissue; T, tumor; CGGA, Chinese Glioma Genome Atlas; TCGA, The Cancer Genome Atlas; ROC, receiver operating characteristic; AUC, area under the curve; PRS, prognostic risk score; IDH, isocitrate dehydrogenase; MGMT, O-6-methylguanine-DNA methyltransferase; OS, overall survival; WHO, World Health Organization; NC, negative control; si, small interfering RNA; OD, optical density; AO/EB, acridine orange/ethidium bromide; GSEA, Gene Set Enrichment Analysis; PPI, protein-protein interaction; PCNA, proliferating cell nuclear antigen; MCM2/3/4/6, minichromosome maintenance complex component 2/3/4/6; PLK1, polo-like kinase 1; MAD2L1, mitotic arrest deficient 2 like 1; GBM, glioblastoma; LGG, low-grade glioma.

interactions, with Sidak's test employed for multiple comparisons. Correlations were determined using Pearson's correlation coefficient. $P<0.05$ was considered to indicate a statistically significant difference.

Results

Research workflow and sample characteristics. The overall research workflow is summarized in Fig. 1. Based on predefined screening criteria, gene expression profiles (GSE29796, GSE4290, GSE50161 and GSE7696) and corresponding clinical data were retrieved from the GEO database. These datasets included 52, 153, 117 and 80 glioma specimens, respectively, alongside 20, 23, 13 and 4 non-tumorous controls. Clinicopathological information, such as age, tumor grade, histological classification, 1p/19q codeletion and IDH mutation status, was obtained from the CGGA and TCGA databases. Additional data on chemoradiotherapy history and MGMT promoter methylation were available exclusively from the CGGA dataset. Detailed clinical characteristics are provided in Table SI.

Identification of important genes involved in glioma initiation and progression. Gene expression profiles from the GSE29796, GSE4290, GSE50161 and GSE7696 datasets were stratified into tumor and non-tumor groups for differential expression analysis. DEGs were identified using a significance threshold of $P<0.05$ and $|\log_2 FC|>1$. The GSE29796 dataset included 5,715 DEGs (599 upregulated and 5,116 downregulated; Fig. 2A), GSE4290 included 2,450 DEGs (1,425 upregulated and 1,025 downregulated; Fig. 2B), GSE50161 included 4,696 DEGs (2,320 upregulated and 2,376 downregulated; Fig. 2C) and GSE7696 included 1,532 DEGs (915 upregulated and 617 downregulated; Fig. 2D). Intersecting DEGs across all four datasets via a Venn diagram (Fig. 2E) yielded 360 commonly dysregulated genes. A PPI network was generated using STRING and 180 proteins were imported into Cytoscape for visualization. Subsequent topological analysis using the cytoHubba plugin identified CDK1 as the core hub gene with the highest degree value (Fig. 2F).

CDK1 expression level in glioma. CDK1 expression across GEO datasets revealed significantly elevated levels in

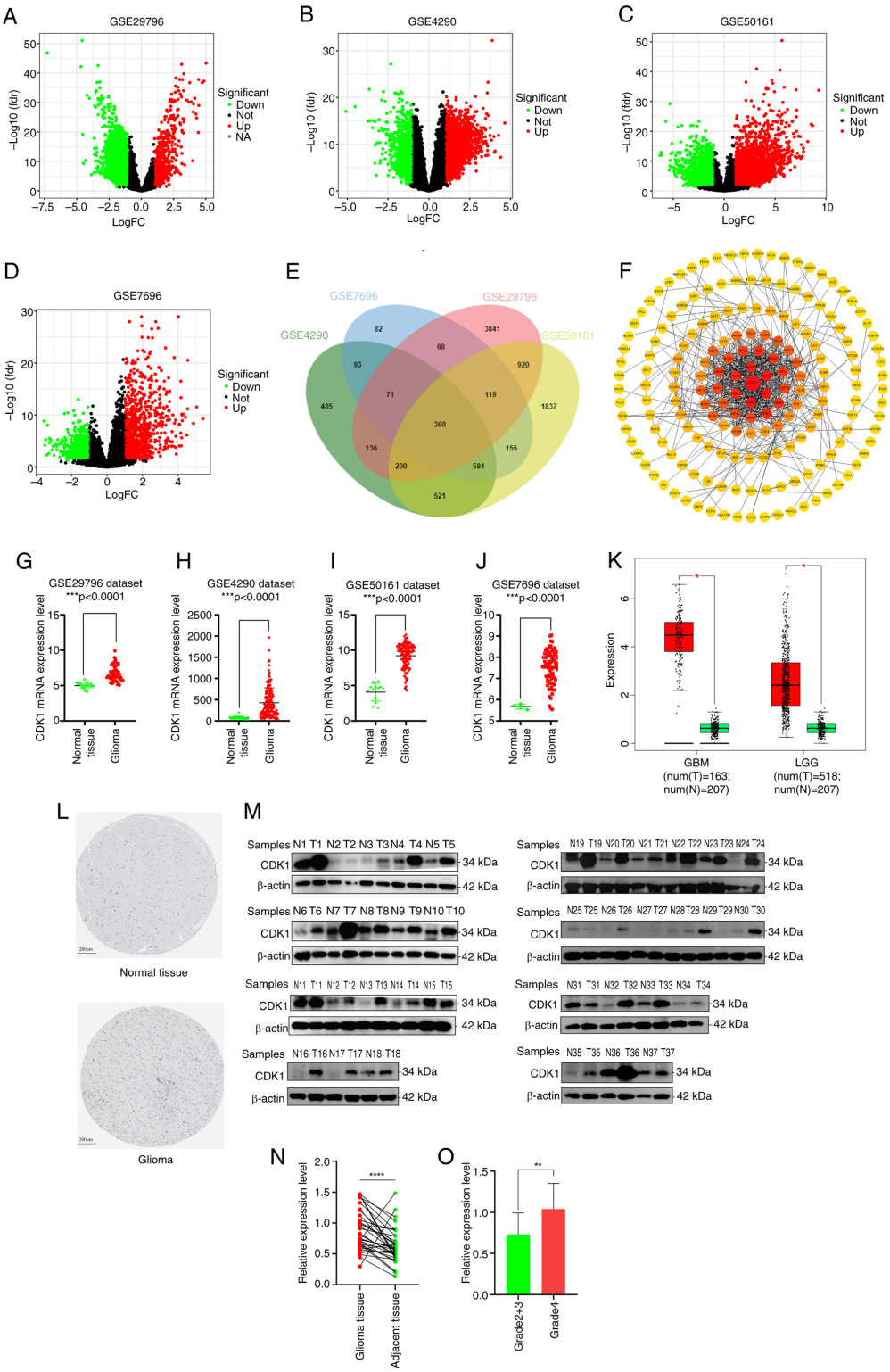

Figure 2. Core gene and its expression levels in normal tissue and glioma were retrieved. (A) Volcano plots of the 5,715 DEGs in the GSE29796 dataset (599 upregulated and 5,116 downregulated). (B) Volcano plots of the 2,450 DEGs in the GSE4290 dataset (1,425 upregulated and 1,025 downregulated). (C) Volcano plots of the 4,696 DEG in the GSE50161 dataset (2,320 upregulated and 2,376 downregulated). (D) Volcano plots of the 1,532 DEGs in the GSE7696 dataset (915 upregulated and 617 downregulated). The red nodes represent the significantly upregulated genes with log2FC>1 and P<0.05. The green nodes represent the significantly downregulated genes with log2FC<-1 and P<0.05. (E) Intersecting genes of the four groups of DEGs are displayed by Venn diagram. (F) Protein-protein interaction network was constructed and the core protein with the highest degree of topology value was screened out, based on the STRING website and Cytoscape visualization software. Comparison of CDK1 mRNA expression levels in normal tissue and glioma using the (G) GSE29796, (H) GSE4290, (I) GSE50161 and (J) GSE7696 datasets. (K) CDK1 expression levels in normal tissue and glioma via GEPIA analysis. (L) The protein levels of CDK1 in normal (intensity: negative; quantity: none) and glioma (intensity: strong; quantity: <25%) tissue from the Human Protein Atlas. (M) Western blot assay and (N) Wilcoxon matched-pairs signed rank test (P<0.0001) of 37 pairs of glioma and adjacent tissues. (O) Data from the internal cohort showed that CDK1 expression was a statistically significant difference between Grade 2+3 gliomas (n=20) and Grade 4 gliomas (n=17) (P=0.0018). Data are presented as mean ± SD. *P<0.05, **P<0.01, ***P<0.001, ****P<0.0001. Statistical significance was calculated using unpaired t-test, Mann Whitney test or Wilcoxon matched-pairs signed rank test. FC, fold change; DEGs, differentially expressed genes; CDK1, cyclin-dependent kinase 1; GEPIA, Gene Expression Profiling Interactive Analysis; N, normal tissue; T, tumor.

glioma tissues relative to the normal controls (Fig. 2G-J). Consistent findings from GEPIA analyses further confirmed upregulated CDK1 expression in both GBM and LGG cohorts (Fig. 2K). Additionally, immunohistochemical data from the HPA database demonstrated significantly higher CDK1 protein abundance in glioma tissues compared with normal brain tissue (Fig. 2L). To experimentally validate these bioinformatic observations, CDK1 protein expression in an internal cohort of 37 paired glioma and adjacent normal tissues was assessed via western blotting. Despite the limited cohort size, the results consistently showed elevated CDK1 protein levels in glioma samples (P<0.0001, paired t-test; Fig. 2M and N). Furthermore, data from the internal cohort showed CDK1 expression was significantly higher in WHO grade 4 gliomas (n=17) than in WHO grade 2+3 gliomas (n=20) (P=0.0018; Fig. 2O).

CDK1 upregulation is combined with a poorer survival and prognosis in patients with glioma. Kaplan-Meier survival analysis of the CGGA dataset revealed significantly reduced OS in patients with high CDK1 expression (log-rank P<0.001; Fig. 3A), findings that were independently validated using the TCGA cohort (P<0.001; Fig. 3B). ROC analysis demonstrated consistent prognostic performance across both datasets. In the CGGA cohort, CDK1 showed predictive value for 1-, 3- and 5-year survival with area under the curves (AUCs) of 0.672, 0.751 and 0.744, respectively (Fig. 3C). Correspondingly, the TCGA dataset yielded AUCs of 0.745, 0.833 and 0.779 for the same time intervals (Fig. 3D). To assess CDK1 as an independent prognostic determinant, univariate and multivariate Cox regression analyses were performed using the CGGA dataset. Univariate analysis identified significant associations between OS and CDK1 expression [hazard ratio (HR), 1.482; 95% confidence interval (CI), 1.386-1.585; P<0.001], as well as progression status, tumor grade, age, IDH mutation and 1p/19q codeletion status (Fig. 3E). Multivariate analysis confirmed CDK1 as an independent prognostic factor (HR, 1.260; 95% CI, 1.173-1.355; P<0.001), alongside progression status, grade, age, chemotherapy, IDH mutation, and 1p/19q codeletion status (Fig. 3G). The emergence of chemotherapy as a significant prognostic factor only in the multivariate analysis indicates that its effect is not independent but becomes evident after accounting for other covariates. This pattern implies that the efficacy of chemotherapy may depend on specific contexts, such as particular molecular subgroups (such as gliomas with MGMT promoter methylation), where a significant benefit might be diluted and non-significant in a heterogeneous cohort under univariate assessment. These associations were validated using the TCGA dataset (Fig. 3F and H). Collectively, these results establish CDK1 as an independent prognostic biomarker for glioma. A prognostic nomogram integrating tumor grade, IDH mutation status, MGMT promoter methylation, 1p/19q codeletion status and CDK1 expression was constructed using the CGGA cohort (Fig. 3I). Among the variables integrated into the nomogram, CDK1 expression was established as a key driver of the predictive power of the model based on variable importance analysis. Calibration plots demonstrated good concordance between predicted and observed survival probabilities, particularly for 3-year OS (Fig. 3J-L).

Relative analysis of CDK1 gene expression and clinicopathological features based on the CGGA dataset. CDK1 expression was significantly elevated in patients >42 years (P=0.002; Fig. 4A) and increased progressively with tumor grade (P<0.001; Fig. 4B). Conversely, significantly lower CDK1 levels were observed in IDH-mutant and 1p/19q codeleted gliomas (both P<0.001; Fig. 4C and D). Recurrent and secondary gliomas exhibited significantly higher CDK1 expression compared with primary tumors (P<0.001; Fig. 4E). Stratification by molecular subtype further revealed CDK1 upregulation in IDH-wild type glioblastomas relative to IDH-mutant astrocytomas and oligodendrogliomas (P<0.001; Fig. 4F). Within the IDH-mutant subgroup, astrocytomas (IDH-mutant, 1p/19q non-codel) displayed higher CDK1 expression than oligodendrogliomas (IDH-mutant, 1p/19q codeleted) (P=0.0305; Fig. 4G), underscoring its subtype-specific regulation.

CDK1 facilitates the malignant biological phenotypes of glioma cells

Construction of glioma cells line with CDK1 knockdown. To investigate CDK1 function, U251MG and LN229 glioma cell lines were transiently transfected with sequence-specific CDK1 siRNA. Western blot analysis confirmed the efficient knockdown of CDK1 protein expression in both the U251MG and LN229 cell lines transfected with CDK1-siRNA, compared with the Blank and negative control (NC) groups (P<0.05; Fig. 5A-D).

CDK1 positively regulates the cell proliferative ability of glioma cells. CCK-8 assays demonstrated that CDK1 knockdown significantly suppressed proliferation in both U251MG and LN229 cells (P<0.001; Fig. 5E and F). EdU fluorescence staining confirmed that proliferation was significantly reduced in the CDK1-siRNA group compared with the NC (U251: P=0.0325; Fig. 5G and H) (LN229: P=0.0057; Fig. 5I and J). These results establish CDK1 as a potential promoter of glioma cell proliferation.

CDK1 enhances the migration and invasive abilities of glioma cells. Transwell migration assays revealed a significant reduction in migrated cell counts following CDK1 knockdown (U251: P<0.001; Fig. 6A and B) (LN229: P=0.0002; Fig. 6C and D). Similarly, Matrigel invasion assays demonstrated significant suppression of invasive potential in CDK1-siRNA cells (U251: P<0.001; Fig. 6E and F) (LN229: P=0.0003; Fig. 6G and H). Scratch wound healing assays in U251MG cells confirmed progressive inhibition of migration at 48 and 72 h post-transfection (P=0.0027 and P<0.0001, respectively; Fig. 6I and J). Collectively, these findings underscore the role of CDK1 in driving glioma cell motility and invasiveness.

CDK1 inhibits glioma cell apoptosis. Flow cytometry analysis revealed that RNA interference-mediated CDK1 knockdown resulted in a 7-fold increase in apoptosis relative to the NC group (P<0.001; Fig. 6K and L). AO/EB staining, a dual-fluorescence apoptosis assay, exploits the ability of AO to permeate intact membranes, intercalate with nuclear DNA and emit bright green fluorescence. By contrast, EB penetrates only cells with compromised membranes, binds nuclear DNA and produces orange-red fluorescence. Accordingly, apoptotic cells exhibit uniform, condensed or fragmented red-orange fluorescent nuclei, whereas viable cells display diffuse green

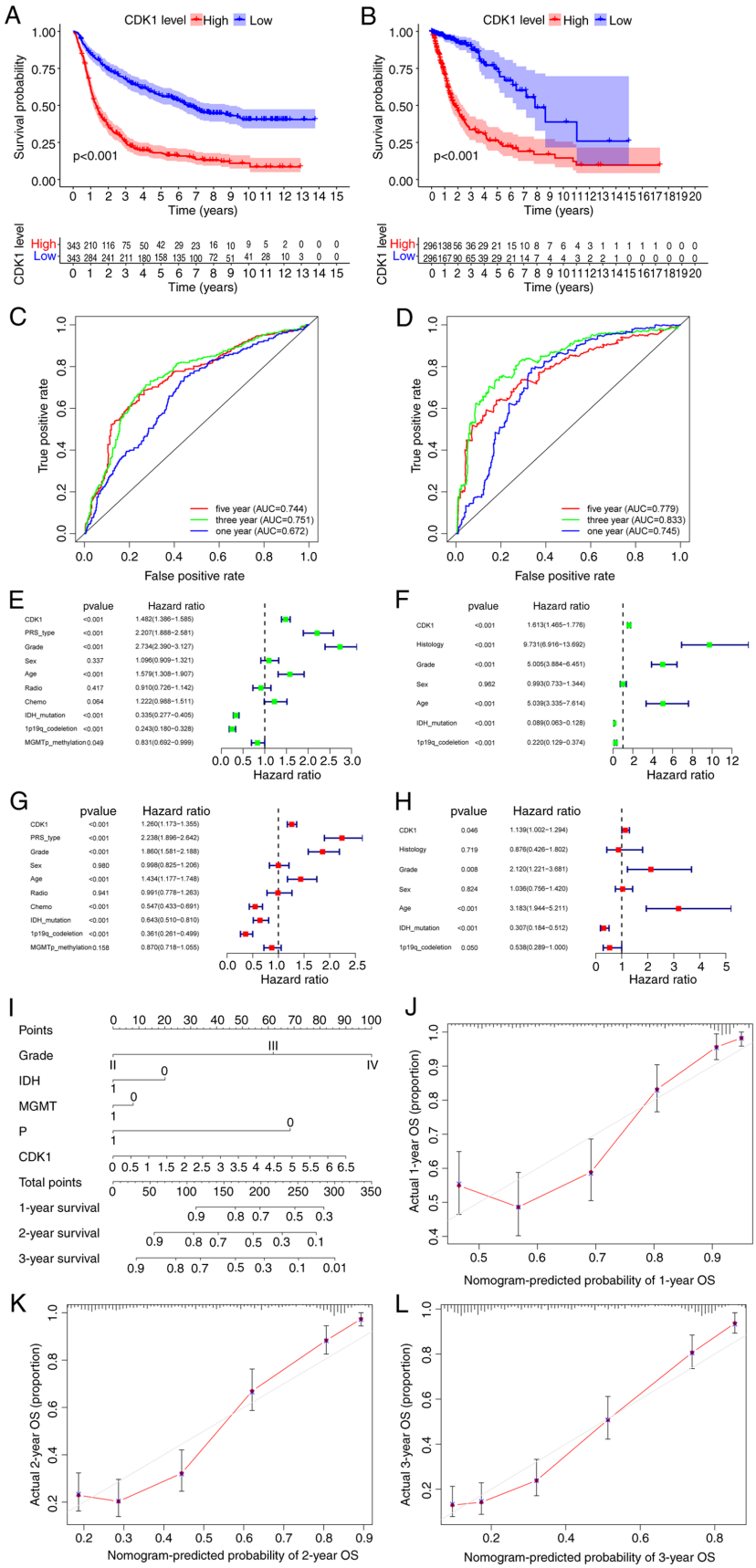

Figure 3. Survival analysis and independent prognostic analysis of CDK1 based on bioinformatics analysis. Survival analysis of the high and low CDK1 groups in patients with glioma from the (A) CGGA and (B) TCGA datasets. The ROC curves of CDK1 at 1, 3 and 5 year survival in the (C) CGGA and (D) TCGA datasets. Univariate analysis of CDK1 in the (E) CGGA and (F) TCGA datasets. Multivariate analysis of CDK1 in the (G) CGGA and (H) TCGA datasets. (I) Prognostic nomogram constructed based on the CGGA dataset including clinical information to predict the survival of patients with glioma. Calibration curves of the nomogram constructed based on the CGGA dataset to predict survival at (J) 1 year, (K) 2 years and (L) 3 years. CDK1, cyclin-dependent kinase 1; CGGA, Chinese Glioma Genome Atlas; TCGA, The Cancer Genome Atlas; ROC, receiver operating characteristic; AUC, area under the curve; PRS, prognostic risk score; IDH, isocitrate dehydrogenase; MGMT, O-6-methylguanine-DNA methyltransferase; OS, overall survival.

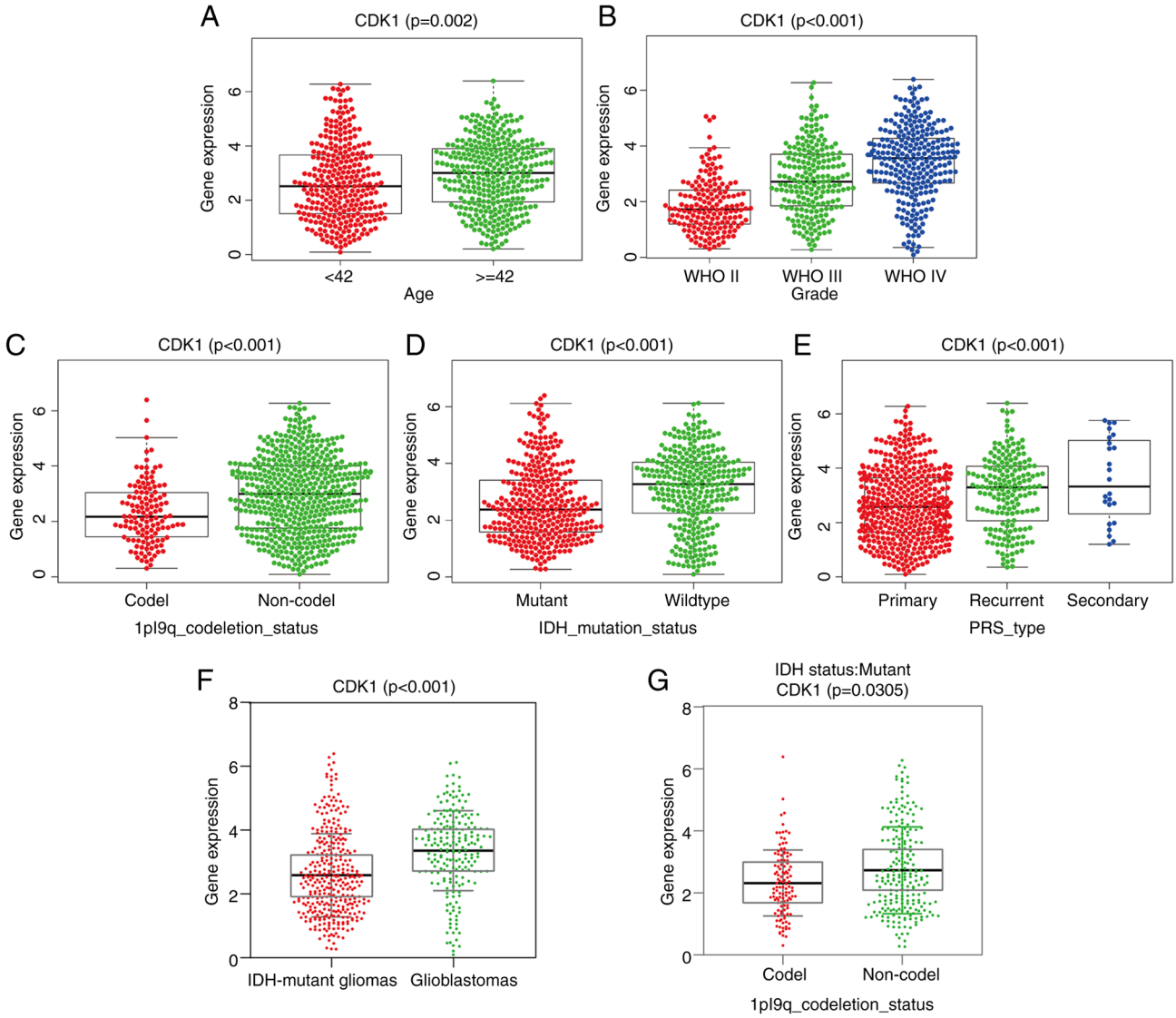

Figure 4. Association between CDK1 and the clinicopathological characteristics of patients with glioma in the Chinese Glioma Genome Atlas dataset. (A) The CDK1 expression level by age (≥42 vs. <42 years; P=0.002). (B) The CDK1 expression level by glioma grade (WHO II, III and IV; P<0.001). (C) The CDK1 expression level by 1p19q codeletion status (codel vs. non-codel; P<0.001). (D) The CDK1 expression level by IDH mutation state (mutant vs. wild-type; P<0.001). (E) The CDK1 expression level by glioma type (primary, recurrent and secondary; P<0.001). (F) The CDK1 expression level in IDH-wildtype glioblastoma vs. IDH-mutant astrocytoma and oligodendroglioma (P<0.001). (G) The CDK1 expression level in IDH-mutant astrocytoma (1p/19q non-codel) vs. IDH-mutant oligodendroglioma (1p/19q code) (P=0.0305). Data are presented as mean ± SD. Statistical significance was calculated using unpaired t-test or Mann Whitney test. CDK1, cyclin-dependent kinase 1; WHO, World Health Organization; IDH, isocitrate dehydrogenase.

fluorescence. AO/EB staining of U251MG and LN229 glioma cells demonstrated significantly increased red fluorescence in siRNA-treated groups, corresponding to 3.2-fold and 4.4-fold elevations in apoptotic rates, respectively (U251MG: P=0.0089; LN229: P=0.0143; Fig. 6M-P). These findings collectively confirm that CDK1 suppression significantly enhanced apoptosis in glioma cells.

CDK1 boosts DNA damage repair ability in glioma cells. X-ray-induced DNA double-strand break (DSB) repair following 5 Gy irradiation was evaluated using γ-H2AX immunofluorescence (Fig. 6Q and R). Quantitative analysis in U251MG cells (Fig. 6S) revealed that the siRNA group displayed significantly slower kinetics of γ-H2AX foci disappearance, indicative of impaired DSB repair, compared with the NC group at all time points: 0.5 h (P<0.0001), 2 h (P<0.0001), 6 h (P<0.0001) and 24 h (P=0.0065). The resolution of the γ-H2AX signal primarily involves the dephosphorylation of γ-H2AX and the disassembly of repair protein complexes at the damage site, which occurs upon successful DSB repair. Therefore, the prolonged presence of γ-H2AX foci in the siRNA group suggests a deficiency in completing the repair process. Consistent results were obtained in LN229 cells under identical conditions (Fig. 6T): 0.5 h (P=0.0017), 2 h (P<0.0001), 6 h (P<0.0001) and 24 h (P=0.0470). CDK1 knockdown by siRNA significantly impaired DSB repair fidelity, linking its role in cell cycle regulation to enhanced DNA damage response and radiation resistance.

DEG analysis and signal pathway enrichment analysis of the CDK1 gene. Using the median CDK1 expression value to stratify samples into high- and low-expression groups, subsequent differential expression analysis comparing these

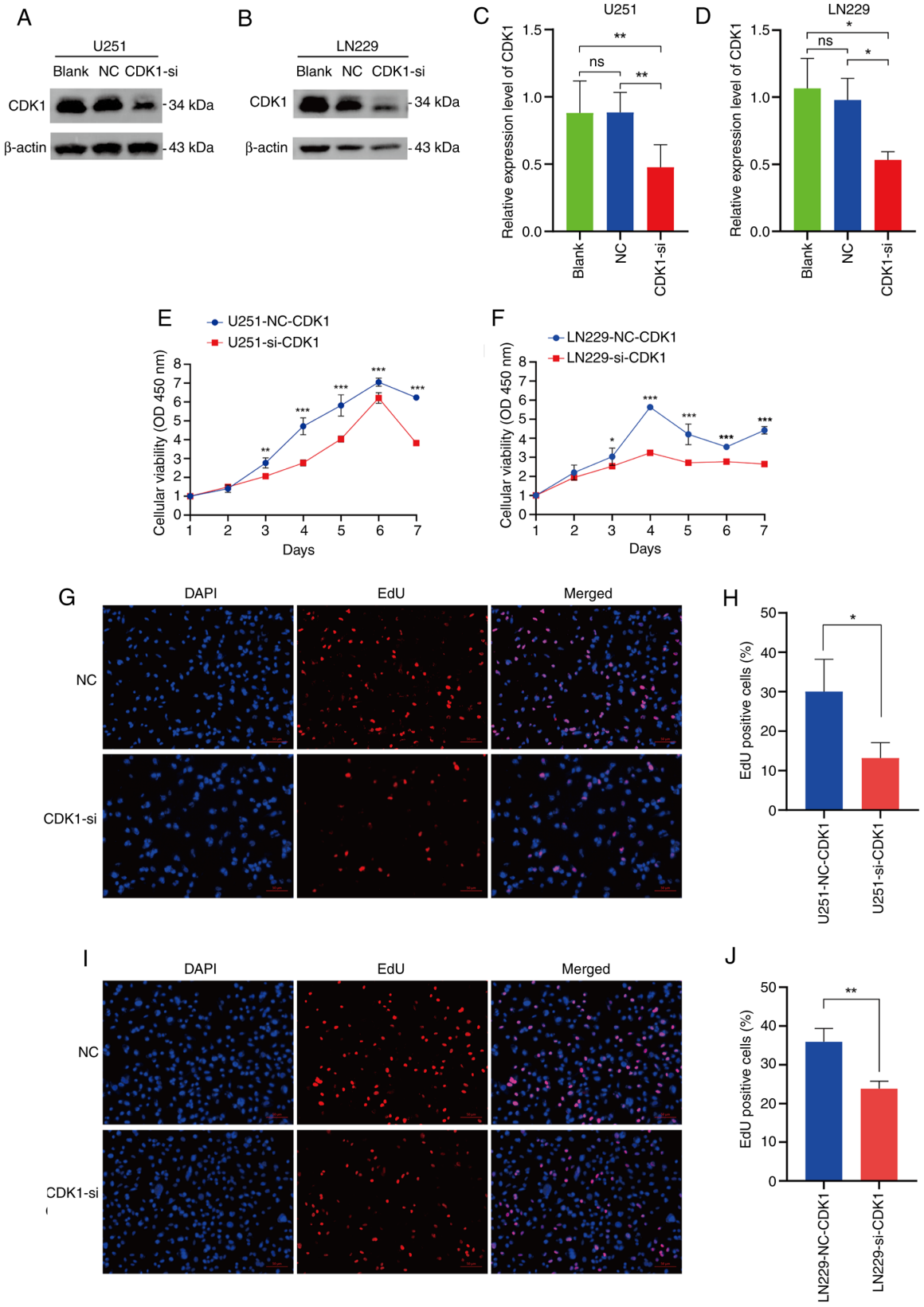

Figure 5. Verification of CDK1 knockdown and its role in the proliferative ability of glioma cells. Validation of CDK1 knockdown was achieved through western blot analysis in the (A) U251MG and (B) LN229 glioma cell lines. (C and D) Statistical comparisons of the western blot data for the (C) U251MG (Blank vs. NC, P=0.9992; Blank vs. CDK1-si, P=0.0057; NC vs. CDK1-si, P=0.0053) and LN229 (Blank vs. NC, P=0.7960; Blank vs. CDK1-si, P=0.0161; NC vs. CDK1-si, P=0.0343) cell lines (n=3, each group). (E and F) Cell Counting Kit-8 cell viability assays demonstrated a decrease in proliferation potential upon CDK1 knockdown in (E) U251MG and (F) LN229 cells (n=4, each group). (G) Representative images (magnification, x10) and (H) quantitative analysis of the EdU assay performed in the U251MG cell line (NC vs. CDK1-si, P=0.0325; n=3, each group). (I) Representative images (magnification, x10) and (J) quantitative analysis of the EdU assay performed in the LN229 cell line (NC vs. CDK1-si, P=0.0057; n=3, each group). Data are presented as mean ± SD. Statistical significance was calculated using one-way analysis of variance followed by Tukey's multiple comparisons test, unpaired t-test or one-way analysis of variance followed by Sidak's multiple comparisons test. *P<0.05, **P<0.01, ***P<0.001. CDK1, cyclin-dependent kinase 1; NC, negative control; si, small interfering (RNA); OD, optical density.

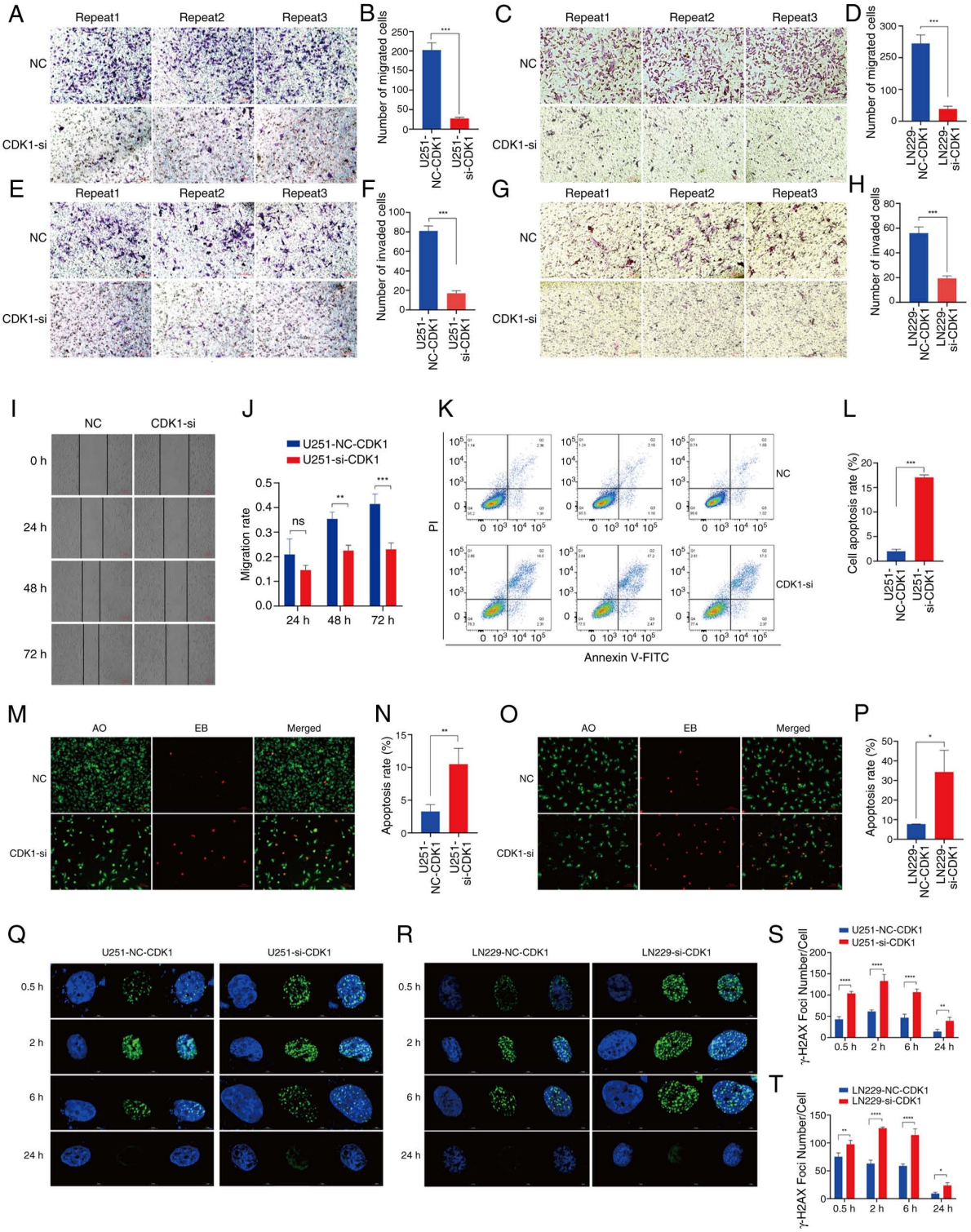

Figure 6. Impact of CDK1 on the migration/invasion capability and DNA damage repair ability of glioma cells. (A) Representative images of the U251MG cell Transwell migration assay (magnification, x10) and the (B) quantitative analysis of the number of migrated cells (NC vs. CDK1-si, P<0.001; n=3). (C) Representative images of the LN229 cell Transwell migration assay (magnification, x10) and the (D) quantitative analysis of the number of migrated cells (NC vs. CDK1-si, P=0.0002; n=3). (E) Representative images of the U251MG cell Transwell invasion assay (magnification, x10) and the (F) quantitative analysis (NC vs. CDK1-si, P<0.001; n=3). (G) Representative images of the LN229 cell Transwell invasion assay (magnification, x10) and the (H) quantitative analysis (NC vs. CDK1-si, P=0.0003; n=3). (I) The assessment of cell migration via scratch experiments demonstrated a significant effect of CDK1 knockdown on reducing glioma cell motility. (J) Statistical results of the U251MG cell line migration assay (NC vs. CDK1-si, 24 h P=0.1445; 48 h P=0.0027; 72 h P=0.0001; n=3). (K and L) Analysis of apoptosis by flow cytometry using Annexin V-FITC and PI staining in U251MG cells. (K) Representative dot plots and (L) quantitative analysis (NC vs. CDK1-si, P<0.001; n=3). (M and N) Detection of apoptosis by AO/EB fluorescence staining in U251MG cells. (M) Representative fluorescence images (magnification, x10) and the (N) quantitative analysis (NC vs. CDK1-si, P=0.0089; n=3). (O and P) Detection of apoptosis by AO/EB fluorescence staining in LN229 cells. (O) Representative fluorescence images (magnification, x10) and the (P) quantitative analysis (NC vs. CDK1-si, P=0.0143; n=3). Images of γ-H2AX foci formed in (Q) U251MG and (R) LN229 cell lines at 0.5, 2, 6 and 24 h after 5 Gy radiation. The statistical analysis of γ-H2AX foci formed in (S) U251MG and (T) LN229 cell lines (NC vs. CDK1-si; n=3). Data are presented as mean ± SD. Statistical significance was calculated using unpaired t-test or one-way analysis of variance followed by Sidak's multiple comparisons test. *P<0.05, **P<0.01, ***P<0.001, ****P<0.0001. ns, not significant. CDK1, cyclin-dependent kinase 1; NC, negative control; si, small interfering (RNA); AO/EB, acridine orange/ethidium bromide.

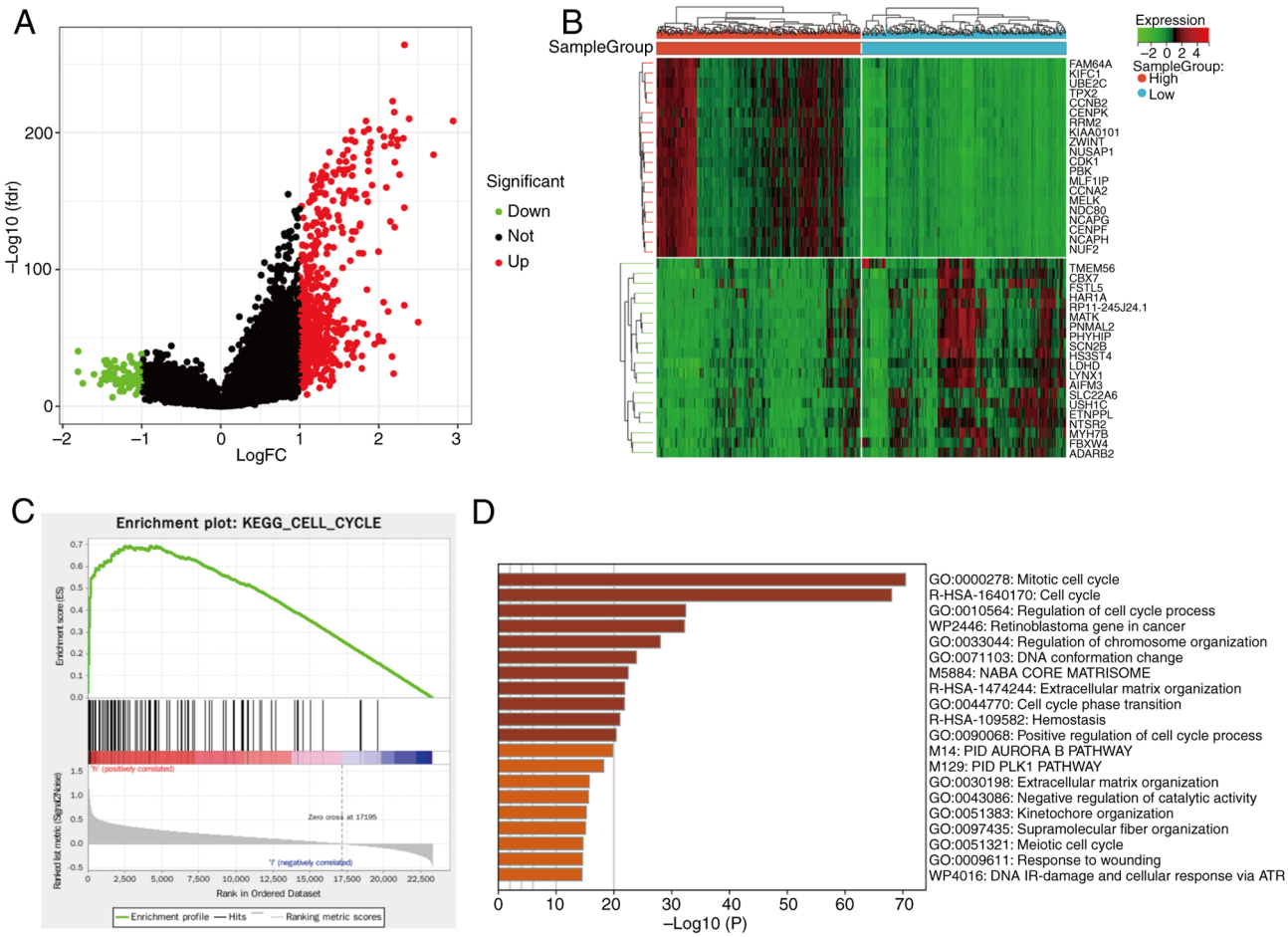

Figure 7. DEG analysis and pathway enrichment analysis of the CDK1 gene based on Chinese Glioma Genome Atlas dataset. (A) Volcano plots of DEGs. The red nodes represent the significantly upregulated genes with log2FC>1 and P<0.05. The green nodes represent the significantly downregulated genes with log2FC<-1 and P<0.05. (B) Heatmap of DEGs indicating the significantly upregulated and significantly downregulated DEGs. (C) Enriched cell cycle signaling pathway by Gene Set Enrichment Analysis. (D) Heatmap of pathway enrichment analysis across DEGs based on Metascape analysis. FC, fold change; DEG, differentially expressed gene; CDK1, cyclin-dependent kinase 1.

two groups yielded 638 DEGs, including 93 upregulated and 546 downregulated genes. A volcano plot of DEGs was generated using R software (Fig. 7A), and a heatmap illustrated the most significantly altered genes (Fig. 7B). KEGG pathway enrichment analysis revealed significant enrichment of cell cycle-related pathways in the high-CDK1 expression group (NES=2.0351, normalized P<0.05, FDR=0.0101; Fig. 7C). Consistently, Metascape analysis indicated strong enrichment of DEGs in the 'mitotic cell cycle' pathway (Fig. 7D).

Core genes highly associated with CDK1 and PPI network in the cell cycle pathway. Both GSEA and Metascape enrichment analyses highlighted convergence on cell cycle-associated pathways. Venn diagram intersection identified 29 overlapping genes from the two analyses (Fig. 8A). To identify core regulators associated with CDK1, these genes were uploaded to STRING for PPI network analysis, which was visualized in Cytoscape. In total, 8 hub proteins exhibiting strong co-expression with CDK1 (correlation >0.9) were identified: PCNA, MCM2, MCM3, MCM4, MCM6, PLK1, TTK and MAD2L1 (Fig. 8B). STRING-based PPI analysis confirmed robust interconnectivity among these proteins (Fig. 8C, top), and correlation analysis further demonstrated strong positive associations between CDK1 and the 8 hub genes (Fig. 8C, bottom), corroborated by scatter plots (Fig. 8D-K). Univariate regression analysis revealed that all 8 genes functioned as oncogenic drivers in glioma (P<0.001; Fig. 8L).

Malignant phenotypes are promoted through modulation of the cell cycle pathway via influencing CDK1 expression

Hub gene survival and prognosis analysis based on TCGA dataset. In glioma tissues, expression levels of the identified hub genes were significantly elevated relative to normal tissues, and their upregulation was associated with a poor OS (Fig. 9A-H).

Suppression of CDK1 expression can inhibit the cell cycle pathway, thereby downregulating the malignant phenotypes of tumors. qPCR confirmed that CDK1 knockdown suppressed the expression of PCNA, MCM2, MCM3, MCM4, MCM6, PLK1 and MAD2L1, providing mechanistic evidence that CDK1 inhibition disrupts cell cycle progression (Fig. 9I-O).

Discussion

Glioma constitutes the most common primary malignant tumor of the brain and is classified into localized and diffuse

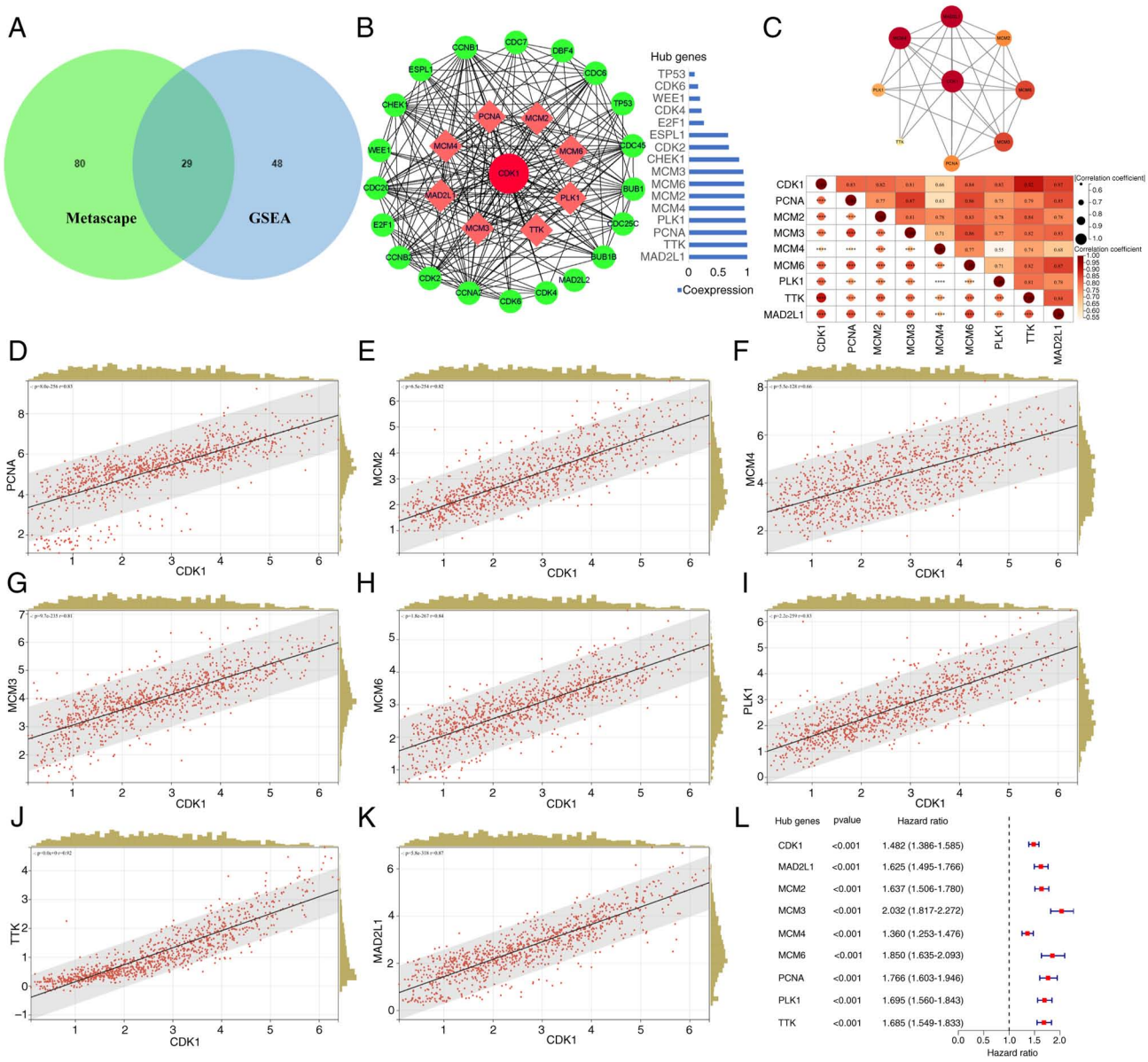

Figure 8. Association analysis between CDK1 and cell cycle hub genes. (A) Intersecting genes of the cell cycle signaling pathway-related genes from Metascape analysis and GSEA are displayed by the Venn diagram. (B) CDK1 PPI network was constructed and the top 8 hub proteins with a co-expression value of >0.9 were screened out based on the STRING website and Cytoscape visualization software. (C) STRING-based PPI analysis among the top 8 hub proteins (top). Matrix correlation analysis and visualization of CDK1 and hub genes (bottom). Scatter plot analysis of the correlation between CDK1 and hub genes expression: (D) PCNA, (E) MCM2, (F) MCM4, (G) MCM3, (H) MCM6, (I) PLK1, (J) TTK and (K) MAD2L1. (L) Univariate regression analysis of the top 8 Hub genes. Statistical significance was calculated using Pearson's correlation coefficient. CDK1, cyclin-dependent kinase 1; GSEA, Gene Set Enrichment Analysis; PPI, protein-protein interaction; PCNA, proliferating cell nuclear antigen; MCM2/3/4/6, minichromosome maintenance complex component 2/3/4/6; PLK1, polo-like kinase 1; MAD2L1, mitotic arrest deficient 2 like 1.

subtypes (40). In contrast to localized gliomas, which are often completely resectable and potentially curable, diffuse gliomas are frequently incompletely resectable due to their infiltrative growth and high malignancy, properties that confer extreme aggressiveness, particularly in high-grade forms (12). Among them, GBM represents the most prevalent and lethal high-grade glioma, accounting for 57% of all gliomas and 48% of primary CNS malignancies (41). The standard therapeutic regimen combines postoperative radiotherapy with temozolomide-based chemotherapy. In recent years, alternating current field therapy (TTF) has been incorporated into National Comprehensive Cancer Network (NCCN) guidelines; however, patient outcomes remain poor (42). The evolving WHO classification of CNS tumors, from 2016 to 2021, has integrated molecular biomarkers, revolutionizing glioma diagnostics and therapeutic stratification (5,43). This paradigm shift underscores the need for diagnostic strategies that accurately capture tumor biology. In this context, serum metabolic profiling has emerged as a promising liquid biopsy approach for brain tumors. This method exploits the partial permeability of the blood-brain barrier to small-molecule metabolites, enabling non-invasive detection of tumor-derived metabolic signatures. Among recent innovations, nanoparticle-enhanced laser desorption/ionization mass spectrometry (NPELDI-MS) represents a major advance. A study has demonstrated its ability to characterize metabolic signatures in brainstem

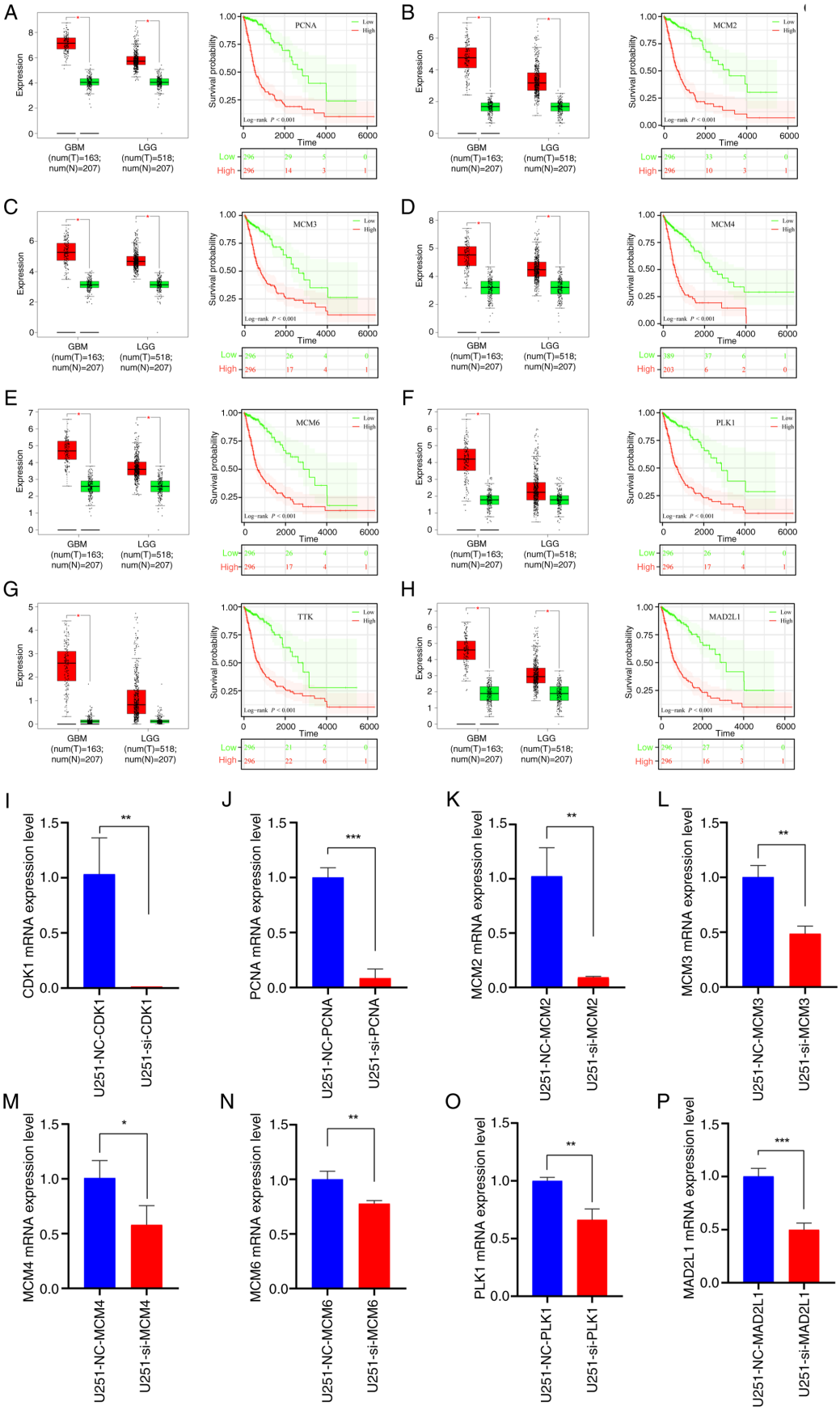

Figure 9. Expression of the top 8 hub genes and prognostic analysis. Expression level of the hub genes in glioma and normal tissues based on the TCGA dataset alongside survival analysis curves for (A) PCNA, (B) MCM2, (C) MCM3, (D) MCM4, (E) MCM6, (F) PLK1, (G) TTK and (H) MAD2L1. (I-P) Quantitative PCR results following CDK1 knock down (n=3) of (I) CDK1, (J) PCNA, (K) MCM2, (L) MCM3, (M) MCM4, (N) MCM6, (O) PLK1 and (P) MAD2L1. Data are presented as mean ± SD. Statistical significance was calculated using log-rank test or Student's t-test. *P<0.05, **P<0.01, ***P<0.001. PCNA, proliferating cell nuclear antigen; MCM2/3/4/6, minichromosome maintenance complex component 2/3/4/6; PLK1, polo-like kinase 1; MAD2L1, mitotic arrest deficient 2 like 1; GBM, glioblastoma; LGG, low-grade glioma; NC, negative control; si, small interfering (RNA); CDK1, cyclin-dependent kinase 1.

gliomas with high diagnostic accuracy (AUC=0.933) and significant prognostic value. Moreover, NPELDI-MS facilitates longitudinal monitoring of treatment response through serial blood sampling, offering a powerful adjunct to conventional imaging and histopathology (44). Despite rapid progress in immunotherapy and targeted therapy, most patients with glioma remain unresponsive due to the complex biology of the tumor and the unique microenvironment of the brain (11,45). Consequently, the systematic identification of novel molecular targets remains an urgent priority in glioma research.

The findings of the present study provide compelling evidence that CDK1 acts as a critical driver of glioma progression. Its upregulation is significantly associated with higher tumor grades, poorer survival and unfavorable prognosis, aligning with reports implicating CDK1 in oncogenic regulation of the cell cycle (46,47). Notably, the present study demonstrated that CDK1 expression was markedly elevated in high-grade gliomas and in patients >42 years of age, suggesting its potential as a biomarker for disease severity and progression. This age-dependent upregulation may reflect the accumulation of genetic and epigenetic alterations promoting CDK1 dysregulation, consistent with emerging insights into age-related oncogenesis (48). These findings emphasize the importance of exploring age-specific molecular mechanisms in glioma, which could reveal novel therapeutic opportunities for older patients who typically experience poorer outcomes (49). In the present study, at the molecular level, the reduced CDK1 expression observed in IDH-mutant and 1p/19q codeleted gliomas highlights the heterogeneity of glioma subtypes and their distinct molecular profiles. This pattern is consistent with evidence that IDH mutations and 1p/19q codeletion confer more favorable prognosis and altered cell cycle regulation (5,50,51). Conversely, the elevated CDK1 levels in recurrent and secondary gliomas underscore its role in tumor relapse and progression, possibly by enhancing proliferation, survival and therapy resistance (52). This is particularly significant given the paucity of effective treatments for recurrent gliomas (53). In the present study, functional assays, including CCK8, EdU, wound healing, Transwell, AO/EB and flow cytometry, demonstrated that CDK1 knockdown markedly inhibited glioma cell proliferation and migration/invasion while promoting apoptosis. The suppression of migration and invasion following CDK1 depletion may involve modulation of epithelial-mesenchymal transition (EMT), a process governed by transcription factors such as TWIST1 and SNAI2 (54). Although direct evidence linking CDK1 to EMT regulation in glioma remains limited, a study on head and neck squamous cell carcinomas indicates that CDK1 can enhance EMT by modulating these key regulators (55). Therefore, we hypothesize that CDK1 knockdown may attenuate glioma cell invasiveness at least partly through EMT inhibition, a hypothesis warranting further mechanistic investigation (56). Collectively, these results reinforce the established role of CDK1 in cell cycle control and underscore its oncogenic potential (15).

In the present study, the dynamic attenuation of γ-H2AX foci observed in U251MG and LN229 cell lines following 5 Gy X-irradiation underscores the pivotal role of CDK1 in maintaining DNA DSB repair fidelity. siRNA-mediated depletion of CDK1 markedly delayed γ-H2AX signal resolution across sequential post-irradiation intervals (0.5-24 h), indicating impaired DSB repair kinetics. Conversely, the NC control group preserved rapid and precise repair, demonstrating the contribution of basal CDK1 activity to radiation resistance. These findings reinforce the established paradigm that CDK1 orchestrates G2/M checkpoint activation and DNA damage response signaling, primarily through phosphorylation of homologous recombination mediators such as BRCA1 and CtBP-interacting protein (CtIP) (57).

The molecular function of CDK1 extends beyond cell cycle regulation to encompass a direct role in DSB repair. A study has demonstrated preferential localization of CDK1-cyclin complexes at DSB sites, where phosphorylation of resection mediators (particularly CtIP and replication protein A 32 kDa subunit) facilitates efficient homologous recombination-mediated repair (57). This kinase activity is essential for resolving replication-associated damage, as CDK1 inhibition disrupts replication fork progression and exacerbates genomic instability (58). The delayed γ-H2AX attenuation observed in CDK1-depleted cells likely reflects defective homologous recombination-repair, consistent with the requirement of CDK1-dependent phosphorylation of BRCA1 at Ser1497 for effective RAD51 recruitment and strand invasion (59).

In the present study, KEGG and GSEA pathway analyses further revealed that CDK1 exerts its principal regulatory effects through the cell cycle pathway, consistent with its established role as a master regulator of mitosis and cell division (60). Notably, a CDK1-centered regulatory network encompassing PCNA, minichromosome maintenance complex components (MCM2/3/4/6), PLK1, TTK and MAD2L1 was delineated, which are key effectors that collectively maintain DNA replication fidelity, checkpoint integrity and chromosomal stability (61-63). Concomitant upregulation of these effectors in gliomas is significantly correlated with reduced OS, highlighting the potential central pathogenetic role of CDK1 (64,65). In the present study, qPCR validation confirmed marked downregulation of these network components following CDK1 depletion, mechanistically linking CDK1 inhibition to cell cycle disruption and revealing its therapeutic potential in glioma management. This mechanistic insight is particularly noteworthy as it not only substantiates the canonical function of CDK1 in cell cycle control but also identifies downstream effectors that may represent additional therapeutic targets. For example, the MCM family, critical for DNA replication initiation and elongation, has recently emerged as a promising target in cancer therapy (66). Likewise, PLK1, a key mitotic kinase implicated in glioma progression, is currently undergoing evaluation in clinical trials (67). Collectively, these findings establish an integrated model of CDK1-centric regulatory topology in gliomagenesis, advocating combinatorial therapeutic strategies targeting multiple interconnected network nodes.

Previous research has consistently demonstrated that activation of CDK family members critically drives tumor cell cycle progression during oncogenesis. Several CDK inhibitors have already received FDA approval (13). For instance, CDK4/6 inhibitors selectively target CDK4 and CDK6 to prevent retinoblastoma protein phosphorylation, thereby halting G1-S transition through inhibition of E2F-dependent gene transcription (68). These inhibitors are now widely used to treat patients with metastatic, hormone receptor-positive and HER2-negative

breast cancer (69,70). Similarly, CDK1 upregulation is correlated with a poor prognosis across multiple malignancies (20,21). Knockdown of CDK1 via short hairpin RNA has been shown to increase apoptosis and enhance chemosensitivity in epithelial ovarian cancer cells (21). Therefore, targeted inhibition of CDK1 expression holds notable therapeutic promise for tumor growth suppression, although the precise regulatory mechanisms warrant further elucidation.

Several limitations of the present study merit consideration. First, the analyses primarily relied on public datasets (TCGA and CGGA) and *in vitro* models, necessitating validation *in vivo*. Second, critical clinicopathological covariates, such as MGMT promoter methylation status, were unavailable in the referenced datasets, limiting comprehensive prognostic interpretation. Finally, although several downstream CDK1 effectors were identified, upstream regulatory mechanisms, including the roles of specific cyclins and modulatory kinases such as Wee1, and potential feedback loops governing CDK1 activity in glioma remain undefined. Future studies aimed at elucidating these upstream regulators are essential to construct a fully integrated model of the CDK1 signaling network and to identify synergistic intervention points for therapeutic development.

In conclusion, glioma remains a life-threatening malignancy with a rising global incidence, particularly for diffuse subtypes that pose formidable therapeutic challenges. Despite advances in treatment modalities, OS has shown minimal improvement (12,40). Therefore, identifying novel molecular markers is essential to elucidate oncogenic mechanisms and facilitate the development of targeted therapies. The present study establishes CDK1 as a critical driver of glioma progression, with its upregulation associated with higher tumor grades, increased recurrence risk and poorer patient outcomes. The age-dependent and subtype-specific expression patterns of CDK1 underscore its potential as both a prognostic biomarker and a therapeutic target. Functional analyses confirmed that CDK1 promotes cell cycle dysregulation through predicted direct interactions with core effectors such as PLK1 and the MCM complex, providing a mechanistic rationale for CDK1-targeted glioma therapy. Notably, the findings of the present study emphasize the importance of dissecting age-specific molecular mechanisms in glioma and delineate a CDK1-centric interactome (PCNAMCM/PLK1/TTK/MAD2L1) with high co-targeting potential. Future investigations should focus on the development of selective CDK1 inhibitors and their evaluation in preclinical and clinical settings, particularly in combination with other therapeutic modalities to overcome resistance and improve clinical outcomes.

Acknowledgements

Not applicable.

Funding

The project was supported by Hebei Natural Science Foundation (grant nos. H2023206913 and J230003), Medical Science Research Project of Hebei (grant no. 20230646) and Hebei Provincial Government funded Clinical Medicine Excellent Talents Project (grant no. ZF2025093).

Availability of data and materials

The data generated in the present study may be requested from the corresponding author.

Authors' contributions

YW and HZ conceived and designed the experiments, conducted the experiments, analyzed the data, prepared figures and/or table and authored and/or verified drafts of manuscripts. XH, DZ, LH, HL, TF and SL contributed to data analysis and revised the manuscript. XX conceived and designed the experiments and authored or reviewed drafts of the paper. YW and HZ confirm the authenticity of all the raw data. All authors read and approved the final version of the manuscript.

Ethics approval and consent to participate

All procedures performed in the present study involving human participants were in accordance with the ethical standards of the institutional and/or national research committee and with the 1964 Helsinki Declaration and its later amendments or comparable ethical standards. The present study was approved by the Ethics Committee of The Second Hospital of Hebei Medical University (approval no. 2019-R191). Informed consent to participate was obtained from all participants included in the present study.

Patient consent for publication

Not applicable.

Competing interests

The authors declare that they have no competing interests.

References

1. Ostrom QT, Gittleman H, Truitt G, Boscia A, Kruchko C and Barnholtz-Sloan JS: CBTRUS statistical report: Primary brain and other central nervous system tumors diagnosed in the United States in 2011-2015. Neuro Oncol 20: iv1-iv86, 2018.
2. Rong L, Li N and Zhang Z: Emerging therapies for glioblastoma: Current state and future directions. J Exp Clin Cancer Res 41: 142, 2022.
3. Yu MW and Quail DF: Immunotherapy for glioblastoma: Current progress and challenges. Front Immunol 12: 676301, 2021.
4. Louis DN, Perry A, Reifenberger G, von Deimling A, Figarella-Branger D, Cavenee WK, Ohgaki H, Wiestler OD, Kleihues P and Ellison DW: The 2016 world health organization classification of tumors of the central nervous system: A summary. Acta Neuropathol 131: 803-820, 2016.
5. Louis DN, Perry A, Wesseling P, Brat DJ, Cree IA, Figarella-Branger D, Hawkins C, Ng HK, Pfister SM, Reifenberger G, *et al*: The 2021 WHO classification of tumors of the central nervous system: A summary. Neuro Oncol 23: 1231-1251, 2021.
6. Bruford EA, Braschi B, Denny P, Jones TEM, Seal RL and Tweedie S: Guidelines for human gene nomenclature. Nat Genet 52: 754-758, 2020.
7. Śledzińska P, Bebyn MG, Furtak J, Kowalewski J and Lewandowska MA: Prognostic and predictive biomarkers in gliomas. Int J Mol Sci 22: 10373, 2021.
8. Qu S, Huang C, Zhu T, Wang K, Zhang H, Wang L, Xu R, Zheng H, Yuan X, Liu G, *et al*: OLFML3, as a potential predictor of prognosis and therapeutic target for glioma, is closely related to immune cell infiltration. VIEW 4: 20220052, 2023.

9. Alleman K, Knecht E, Huang J, Zhang L, Lam S and DeCuypere M: Multimodal deep learning-based prognostication in glioma patients: A systematic review. Cancers (Basel) 15: 545, 2023.
10. Yuan Y, Zhang X, Wang Y, Li H, Qi Z, Du Z, Chu YH, Feng D, Hu J, Xie Q, *et al*: Multimodal data integration using deep learning predicts overall survival of patients with glioma. VIEW 5: 20240001, 2024.
11. Xu S, Tang L, Li X, Fan F and Liu Z: Immunotherapy for glioma: Current management and future application. Cancer Lett 476: 1-12, 2020.
12. Yang K, Wu Z, Zhang H, Zhang N, Wu W, Wang Z, Dai Z, Zhang X, Zhang L, Peng Y, *et al*: Glioma targeted therapy: Insight into future of molecular approaches. Mol Cancer 21: 39, 2022.
13. Le Rhun E, Preusser M, Roth P, Reardon DA, van den Bent M, Wen P, Reifenberger G and Weller M: Molecular targeted therapy of glioblastoma. Cancer Treat Rev 80: 101896, 2019.
14. Malumbres M: Cyclin-dependent kinases. Genome Biol 15: 122, 2014.
15. Malumbres M and Barbacid M: Cell cycle, CDKs and cancer: A changing paradigm. Nat Rev Cancer 9: 153-166, 2009.
16. Han Z, Jia Q, Zhang J, Chen M, Wang L, Tong K, He W, Zhang Y, Zhu W, Qin J, *et al*: Deubiquitylase YOD1 regulates CDK1 stability and drives triple-negative breast cancer tumorigenesis. J Exp Clin Cancer Res 42: 228, 2023.
17. Zeng K, Li W, Wang Y, Zhang Z, Zhang L, Zhang W, Xing Y and Zhou C: Inhibition of CDK1 overcomes oxaliplatin resistance by regulating ACSL4-mediated ferroptosis in colorectal cancer. Adv Sci (Weinh) 10: e2301088, 2023.
18. Shen J, Gong X, Tan S, Zhang Y, Xia R, Xu S, Wang S, Zhou H, Jiang Y, Zhao T, *et al*: CDK1 acts as a prognostic biomarker associated with immune infiltration in pan-cancer, especially in gastrointestinal tumors. Curr Med Chem 32: 4836-4857, 2024.
19. Xue J, Song Y, Xu W and Zhu Y: The CDK1-related lncRNA and CXCL8 mediated immune resistance in lung adenocarcinoma. Cells 11: 2688, 2022.
20. Sung WW, Lin YM, Wu PR, Yen HH, Lai HW, Su TC, Huang RH, Wen CK, Chen CY, Chen CJ and Yeh KT: High nuclear/cytoplasmic ratio of Cdk1 expression predicts poor prognosis in colorectal cancer patients. BMC Cancer 14: 951, 2014.
21. Xi Q, Huang M, Wang Y, Zhong J, Liu R, Xu G, Jiang L, Wang J, Fang Z and Yang S: The expression of CDK1 is associated with proliferation and can be a prognostic factor in epithelial ovarian cancer. Tumour Biol 36: 4939-4948, 2015.
22. Zhang C, Elkahloun AG, Robertson M, Gills JJ, Tsurutani J, Shih JH, Fukuoka J, Hollander MC, Harris CC, Travis WD, *et al*: Loss of cytoplasmic CDK1 predicts poor survival in human lung cancer and confers chemotherapeutic resistance. PLoS One 6: e23849, 2011.
23. van Nes JG, Smit VT, Putter H, Kuppen PJ, Kim SJ, Daito M, Ding J, Shibayama M, Numada S, Gohda K, *et al*: Validation study of the prognostic value of cyclin-dependent kinase (CDK)-based risk in Caucasian breast cancer patients. Br J Cancer 100: 494-500, 2009.
24. Piao J, Zhu L, Sun J, Li N, Dong B, Yang Y and Chen L: High expression of CDK1 and BUB1 predicts poor prognosis of pancreatic ductal adenocarcinoma. Gene 701: 15-22, 2019.
25. Jones MJ and Jones MC: Cell cycle control by cell-matrix interactions. Curr Opin Cell Biol 86: 102288, 2024.
26. Lemmens B, Hegarat N, Akopyan K, Sala-Gaston J, Bartek J, Hochegger H and Lindqvist A: DNA replication determines timing of mitosis by restricting CDK1 and PLK1 activation. Mol Cell 71: 117-128.e113, 2018.
27. Ci M, Zhao G, Li C, Liu R, Hu X, Pan J, Shen Y, Zhang G, Li Y, Zhang L, *et al*: OTUD4 promotes the progression of glioblastoma by deubiquitinating CDK1 and activating MAPK signaling pathway. Cell Death Dis 15: 179, 2024.
28. Shi YX, Zhu T, Zou T, Zhuo W, Chen YX, Huang MS, Zheng W, Wang CJ, Li X, Mao XY, *et al*: Prognostic and predictive values of CDK1 and MAD2L1 in lung adenocarcinoma. Oncotarget 7: 85235-85243, 2016.
29. Faienza F, Polverino F, Rajendraprasad G, Milletti G, Hu Z, Colella B, Gargano D, Strappazzon F, Rizza S, Vistesen MV, *et al*: AMBRA1 phosphorylation by CDK1 and PLK1 regulates mitotic spindle orientation. Cell Mol Life Sci 80: 251, 2023.
30. Auvergne RM, Sim FJ, Wang S, Chandler-Militello D, Burch J, Al Fanek Y, Davis D, Benraiss A, Walter K, Achanta P, *et al*: Transcriptional differences between normal and glioma-derived glial progenitor cells identify a core set of dysregulated genes. Cell Rep 3: 2127-2141, 2013.
31. Sun L, Hui AM, Su Q, Vortmeyer A, Kotliarov Y, Pastorino S, Passaniti A, Menon J, Walling J, Bailey R, *et al*: Neuronal and glioma-derived stem cell factor induces angiogenesis within the brain. Cancer Cell 9: 287-300, 2006.
32. Griesinger AM, Birks DK, Donson AM, Amani V, Hoffman LM, Waziri A, Wang M, Handler MH and Foreman NK: Characterization of distinct immunophenotypes across pediatric brain tumor types. J Immunol 191: 4880-4888, 2013.
33. Lambiv WL, Vassallo I, Delorenzi M, Shay T, Diserens AC, Misra A, Feuerstein B, Murat A, Migliavacca E, Hamou MF, *et al*: The Wnt inhibitory factor 1 (WIF1) is targeted in glioblastoma and has a tumor suppressing function potentially by induction of senescence. Neuro Oncol 13: 736-747, 2011.
34. Zhao Z, Zhang KN, Wang Q, Li G, Zeng F, Zhang Y, Wu F, Chai R, Wang Z, Zhang C, *et al*: Chinese glioma genome atlas (CGGA): A comprehensive resource with functional genomic data from Chinese glioma patients. Genomics Proteomics Bioinformatics 19: 1-12, 2021.
35. Cancer Genome Atlas Research Network: Comprehensive genomic characterization defines human glioblastoma genes and core pathways. Nature 455: 1061-1068, 2008.
36. Brat DJ, Verhaak RG, Aldape KD, Yung WK, Salama SR, Cooper LAD, Rheinbay E, Miller CR, Vitucci M, Morozova O, *et al*: Comprehensive, integrative genomic analysis of diffuse lower-grade gliomas. N Engl J Med 372: 2481-2498, 2015.
37. Ritchie ME, Phipson B, Wu D, Hu Y, Law CW, Shi W and Smyth GK: Limma powers differential expression analyses for RNA-sequencing and microarray studies. Nucleic Acids Res 43: e47, 2015.
38. Livak KJ and Schmittgen TD: Analysis of relative gene expression data using real-time quantitative PCR and the 2(-Delta Delta C(T)) method. Methods 25: 402-408, 2001.
39. Zhou Y, Zhou B, Pache L, Chang M, Khodabakhshi AH, Tanaseichuk O, Benner C and Chanda SK: Metascape provides a biologist-oriented resource for the analysis of systems-level datasets. Nat Commun 10: 1523, 2019.
40. Wu L, Chai R, Zhao Z, Wang Q and Jiang T: Role of the tumor microenvironment in shaping IDH-wildtype glioma plasticity, and potential therapeutic strategies. Cancer Biol Med 19: 1423-1427, 2022.
41. Weller M and Le Rhun E: How did lomustine become standard of care in recurrent glioblastoma? Cancer Treat Rev 87: 102029, 2020.
42. Nabors LB, Portnow J, Ahluwalia M, Baehring J, Brem H, Brem S, Butowski N, Campian JL, Clark SW, Fabiano AJ, *et al*: Central nervous system cancers, Version 3.2020, NCCN Clinical practice guidelines in oncology. J Natl Compr Canc Netw 18: 1537-1570, 2020.
43. Humphrey PA, Moch H, Cubilla AL, Ulbright TM and Reuter VE: The 2016 WHO classification of tumours of the urinary system and male genital organs-part B: Prostate and bladder tumours. Eur Urol 70: 106-119, 2016.
44. Li K, Wang R, Gu Z, Weng W, Liu W, Huang Y, Wu J, Zhang Z, Yang S, Su J, *et al*: Serum metabolic profiling enables diagnosis, prognosis, and monitoring for brainstem gliomas. Nat Commun 16: 6108, 2025.
45. Chen R, Smith-Cohn M, Cohen AL and Colman H: Glioma subclassifications and their clinical significance. Neurotherapeutics 14: 284-297, 2017.
46. Xie B, Wang S, Jiang N and Li JJ: Cyclin B1/CDK1-regulated mitochondrial bioenergetics in cell cycle progression and tumor resistance. Cancer Lett 443: 56-66, 2019.
47. Guan T, Li M, Song Y, Chen J, Tang J, Zhang C, Wen Y, Yang X, Huang L, Zhu Y, *et al*: Phosphorylation of USP29 by CDK1 governs TWIST1 stability and oncogenic functions. Adv Sci (Weinh) 10: e2205873, 2023.
48. López-Otín C, Blasco MA, Partridge L, Serrano M and Kroemer G: Hallmarks of aging: An expanding universe. Cell 186: 243-278, 2023.
49. Chatsirisupachai K, Lesluyes T, Paraoan L, Van Loo P and de Magalhães JP: An integrative analysis of the age-associated multi-omic landscape across cancers. Nat Commun 12: 2345, 2021.
50. Wang HY, Tang K, Liang TY, Zhang WZ, Li JY, Wang W, Hu HM, Li MY, Wang HQ, He XZ, *et al*: The comparison of clinical and biological characteristics between IDH1 and IDH2 mutations in gliomas. J Exp Clin Cancer Res 35: 86, 2016.
51. Nambirajan A, Suri V, Kedia S, Goyal K, Malgulwar PB, Khanna G, Panda PK, Gulati S, Garg A and Sharma MC: Paediatric diffuse leptomeningeal tumor with glial and neuronal differentiation harbouring chromosome 1p/19q co-deletion and H3.3 K27M mutation: Unusual molecular profile and its therapeutic implications. Brain Tumor Pathol 35: 186-191, 2018.

52. Wang Q, Bode AM and Zhang T: Targeting CDK1 in cancer: Mechanisms and implications. NPJ Precis Oncol 7: 58, 2023.
53. Liu Y, Zhou F, Ali H, Lathia JD and Chen P: Immunotherapy for glioblastoma: Current state, challenges, and future perspectives. Cell Mol Immunol 21: 1354-1375, 2024.
54. Pećina-Šlaus N, Zottel A, Škripek Ž, Puljko B, Dumančić F, Bukovac A, Jovčevska I and Kafka A: In silico analysis reveals distinct changes in markers of epithelial to mesenchymal transition in glioma subtypes. Biomol Biomed 25: 2712-2736, 2025.
55. Chen H, Hu K, Xie Y, Qi Y, Li W, He Y, Fan S, Liu W and Li C: CDK1 promotes epithelial-mesenchymal transition and migration of head and neck squamous carcinoma cells by repressing ΔNp63α-mediated transcriptional regulation. Int J Mol Sci 23: 7385, 2022.
56. Ren L, Yang Y, Li W, Zheng X, Liu J, Li S, Yang H, Zhang Y, Ge B, Zhang S, *et al*: CDK1 serves as a therapeutic target of adrenocortical carcinoma via regulating epithelial-mesenchymal transition, G2/M phase transition, and PANoptosis. J Transl Med 20: 444, 2022.
57. Ferretti LP, Lafranchi L and Sartori AA: Controlling DNA-end resection: A new task for CDKs. Front Genet 4: 99, 2013.
58. Tozaki Y, Aoki H, Kato R, Toriuchi K, Arame S, Inoue Y, Hayashi H, Kubota E, Kataoka H and Aoyama M: The combination of ATM and Chk1 inhibitors induces synthetic lethality in colorectal cancer cells. Cancers (Basel) 15: 735, 2023.
59. Liao H, Ji F, Geng X, Xing M, Li W, Chen Z, Shen H and Ying S: CDK1 promotes nascent DNA synthesis and induces resistance of cancer cells to DNA-damaging therapeutic agents. Oncotarget 8: 90662-90673, 2017.
60. Suski JM, Braun M, Strmiska V and Sicinski P: Targeting cell-cycle machinery in cancer. Cancer Cell 39: 759-778, 2021.
61. Masai H, Taniyama C, Ogino K, Matsui E, Kakusho N, Matsumoto S, Kim JM, Ishii A, Tanaka T, Kobayashi T, *et al*: Phosphorylation of MCM4 by Cdc7 kinase facilitates its interaction with Cdc45 on the chromatin. J Biol Chem 281: 39249-39261, 2006.
62. de Cárcer G, Venkateswaran SV, Salgueiro L, El Bakkali A, Somogyi K, Rowald K, Montañés P, Sanclemente M, Escobar B, de Martino A, *et al*: Plk1 overexpression induces chromosomal instability and suppresses tumor development. Nat Commun 9: 3012, 2018.
63. Pierantoni GM, Conte A, Rinaldo C, Tornincasa M, Gerlini R, Valente D, Izzo A and Fusco A: Hmga1 null mouse embryonic fibroblasts display downregulation of spindle assembly checkpoint gene expression associated to nuclear and karyotypic abnormalities. Cell Cycle 15: 812-818, 2016.
64. Yang S, Yuan Y, Ren W, Wang H, Zhao Z, Zhao H, Zhao Q, Chen X, Jiang X and Zhang L: MCM4 is a novel prognostic biomarker and promotes cancer cell growth in glioma. Front Oncol 12: 1004324, 2022.
65. Li X, Tao Z, Wang H, Deng Z, Zhou Y and Du Z: Dual inhibition of Src and PLK1 regulate stemness and induce apoptosis through Notch1-SOX2 signaling in EGFRvIII positive glioma stem cells (GSCs). Exp Cell Res 396: 112261, 2020.
66. Deng S, Lu X, Wang X, Liang B, Xu H, Yang D, Cui G, Yonemura A, Paine H, Zhou Y, *et al*: Overexpression of TBX3 suppresses tumorigenesis in experimental and human cholangiocarcinoma. Cell Death Dis 15: 441, 2024.
67. Reda M, Ngamcherdtrakul W, Nelson MA, Siriwon N, Wang R, Zaidan HY, Bejan DS, Reda S, Hoang NH, Crumrine NA, *et al*: Development of a nanoparticle-based immunotherapy targeting PD-L1 and PLK1 for lung cancer treatment. Nat Commun 13: 4261, 2022.
68. Roskoski R Jr: Cyclin-dependent protein serine/threonine kinase inhibitors as anticancer drugs. Pharmacol Res 139: 471-488, 2019.
69. Gao JJ, Cheng J, Bloomquist E, Sanchez J, Wedam SB, Singh H, Amiri-Kordestani L, Ibrahim A, Sridhara R, Goldberg KB, *et al*: CDK4/6 inhibitor treatment for patients with hormone receptor-positive, HER2-negative, advanced or metastatic breast cancer: A US food and drug administration pooled analysis. Lancet Oncol 21: 250-260, 2020.
70. Curigliano G and Loibl S: CDK4/6 inhibitors in breast cancer: One more step towards reduced mortality. Lancet Oncol 21: 191-192, 2020.